MARX GENERATOR CHARGED VIA BIPERIODIC RESONANT CASCADED TRANSFORMERS

Rudolf H. Potter

Submitted to the faculty of the University Graduate School

in partial fulfillment of the requirements

for the degree

Master of Science

in the Department of Physics,

Indiana University

November 2017

Accepted by the Graduate Faculty, Indiana University, in partial fulfillment of the requirements for the degree of Master of Science.

Master's Thesis Committee

Dr. Shyh-Yuan Lee

Dr. David Whittum

Dr. Matthew Shepherd

Dr. W. Michael Snow

November 16, 2017

DEDICATION

This work is dedicated with love to Harrison J. Potter.

ACKNOWLEDGMENTS

First and foremost, I would like to thank Dr. David Whittum for encouraging me to attend USPAS courses and pursue my Master's degree, for acting as my advisor, and for being a wonderful mentor and teacher. I am grateful to Dr. Shyh-Yuan Lee for sponsoring the USPAS masters program through Indiana University, which allowed me this route to a Master's degree, and for serving as the chair of my master's thesis committee. I would also like to thank Matthew Shepherd and W. Michael Snow for serving on my thesis committee. I would like to thank my generous employer Varian Medical Systems and my manager Mark Trail for allowing me to work on my master's degree as part of my training. I would like to thank Dr. Enno Holzenkämpfer for his time and for his help shaping the final drafts of this thesis. I would like to thank my colleague and friend Dr. Dragoş Constantin for his encouragement, help with LaTeX, and for believing in me. I would like to acknowledge Stephen Vanderet for blazing the trail ahead of me on the Varian USPAS Indiana University master's degree and I wish Tegan Johnson all the best on her upcoming work down this same road. I owe a great debt to Susan Winchester and Moya Wright for keeping me on track and going above and beyond keeping me on course during this journey that my thanks can not begin to recompense. I would like to thank my father Dr. James M. Potter for his help choosing this thesis topic and for his help proof reading my math. Most of all, I would like to thank my wonderful wife Dr. Jennifer M. Potter for her love and support and for doing more than her share of the chores during this process.

Rudolf H. Potter

MARX GENERATOR CHARGED VIA BIPERIODIC RESONANT CASCADED TRANSFORMERS

In this work, a novel method for charging solid state Marx generators is described for the first time. We first review the utility of modulators for powering high power microwave devices. The principal of operation of the Marx generator is then described starting with the classic topology and leading to solid state topologies. The concept of a generalized Marx generator is introduced and several methods of charging are discussed. A resonant cascaded transformers topology emerges from this discussion. Resonant modes are discussed and the topology is refined to take advantage of the $\pi/2$ mode leading to the circuit that is the focus of this work. We begin our analysis of this circuit by considering the corresponding infinite biperiodic system and derive the characteristic dispersion relation. Motivation for closing the stopband is discussed and benefits of the $\pi/2$ mode are noted. We proceed next to derive the matrix equation for the corresponding lossless system of coupled oscillators. To test and verify the analytic work, a five cell benchtop prototype of the charging system is built and its resonant modes are determined empirically. Capacitors in odd numbered resonators are each connected to the input of a voltage doubler circuit and high voltage dc is generated. A MOSFET is added to the output of each doubler circuit and pulsed output is demonstrated. A SPICE simulation of the physical circuit is created. The mode frequencies from the simulation are in good agreement with those measured and calculated. A practical high-power design is considered for the E2V/Teledyne MG7095 magnetron and simulated in SPICE.

CONTENTS

CHAPTER 1

INTRODUCTION

High energy particle accelerators use pulses of radio frequency (rf) power to generate the electric fields needed to accelerate charged particles. The rf power, usually in the microwave frequency range, is generated by vacuum electron devices designed for the purpose, often referred to simply as microwave tubes. These microwave tubes include klystrons, magnetrons, gyrotrons, and traveling wave tubes [1]. Due to electron beam space charge density and cathode surface charge density constraints, microwave tubes are high input impedance devices requiring high input voltages to produce high power microwaves. High peak power is needed to create the accelerating fields but high average power is often not needed and so accelerators are commonly operated in pulsed mode. Gridded microwave tubes can be powered from high voltage dc supplies with the rf power switched via a comparatively low voltage grid pulser, but tubes without a grid need high voltage pulses to operate. These high voltage pulses are generated by a power modulator, sometimes referred to simply as a modulator. The function of the modulator is to store energy from its input, usually three phase ac, convert it to a higher voltage, and release it to the microwave tube at the appropriate time. Available electrical switches are generally rated for lower voltages than microwave tubes require. Careful engineering is necessary to create high voltage pulses using switches rated at lower voltage. Often a pulse transformer is used to step up the voltage after it is

switched as shown in Fig. 1.1

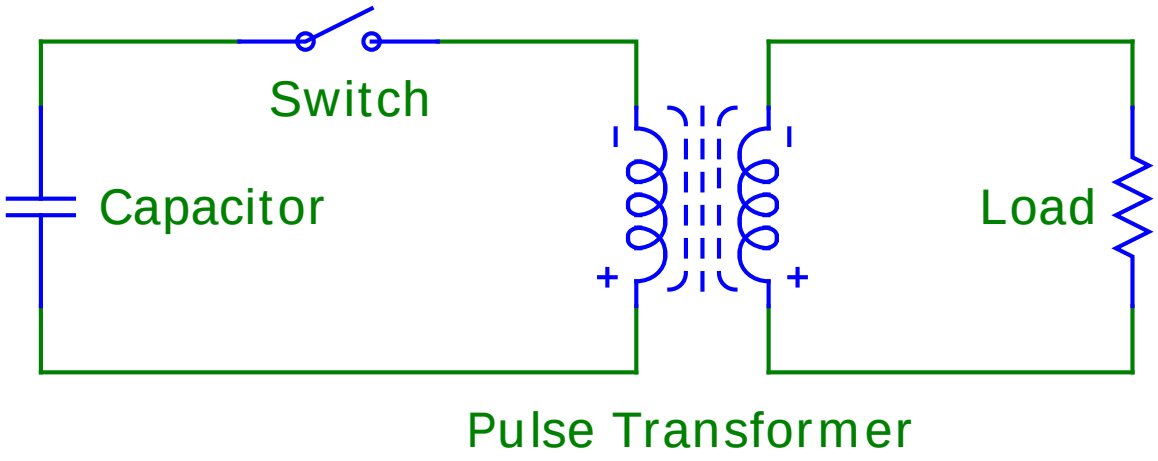

Figure 1.1: Simple modulator with transformer

There are many modulator topologies; they differ mainly in how the designer solved the mismatch between the operating voltage of the switches available and the required voltage that must be delivered to the load. A pulse power modulator design that has received increasing attention in recent years is the solid state Marx generator [2]. The Marx generator is a device for multiplying the voltage from a supply, storing electrical energy, and releasing that energy to a load [3] [4]. The original Marx generator topology, or circuit configuration, was a combination of resistors and capacitors with spark gap switches much like the circuit shown in Fig. 1.2 and was patented by Erwin Otto Marx in 1923 [5]. In this original topology the capacitors are connected to the charging supply through resistors who's resistance is large compared to that of the load. Spark gaps are connected in such a way that when the gaps conduct the capacitors become connected in series with each other and the load. At this point the capacitors are still also connected in parallel to the charging supply but because the charging resistance is much larger than the load resistance little energy is transferred through the charging resistors during the pulse. The discharge occurs when one switch reaches it breakdown point or is triggered. This elevates the voltage on the remaining switches which then breakdown and begin conducting. The pulse ends when the capacitors

are discharged enough that the current in the spark gap is insufficient to keep the plasma hot enough to sustain the arc. Fig. 1.2 shows a classic Marx modulator that is charged through resistors and uses spark gaps as switches to transfer power to the load. The resistor values

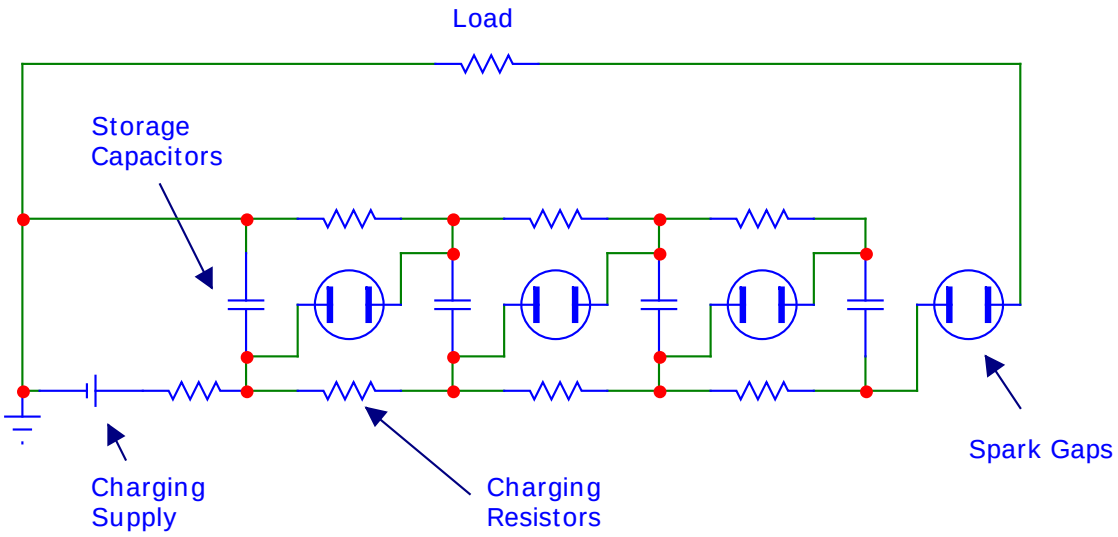

Figure 1.2: Spark gap Marx generator with resistive charging

must be selected to provide a low enough impedance during the charging cycle to allow the capacitors to charge and yet must have a high enough impendence to not drain too much power when the spark gaps conduct. This, and damage to the spark gaps from each pulse, limit the repetition rate for which this topology is useful. There have been improvements to this design such as adding inductors to the charging circuit to improve charging efficiency as in Fig. 1.3. Charging of Marx generators through resistors and inductors is discussed in [6]. In [7], it was shown that the charging time of an inductively charge Marx generator could be decreased by an order of magnitude by coupling the inductors of neighboring stages. To increase the repetition rate of Marx generators further, increase charging efficiency, and allow for output pulse with variable width, the charging resistors/inductors and discharging spark gaps can be replaced with switches as shown in Fig. 1.4.

In principle, any type of switch can be used, even relays, but for modern, high repetition rate designs, solid state transistor switches such as MOSFETs and IGBTs are common.

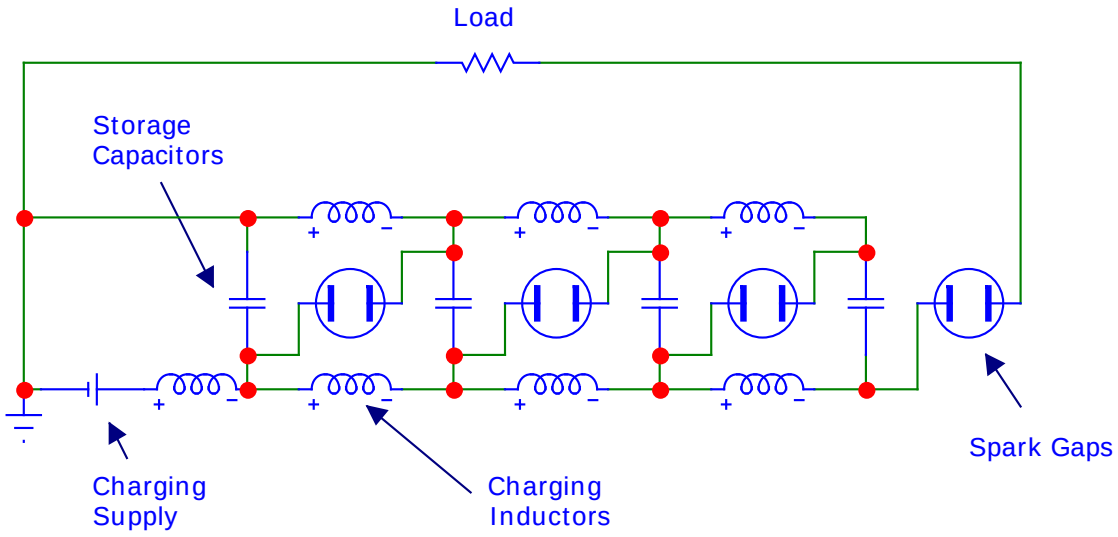

Figure 1.3: Spark gap Marx generator with inductive charging

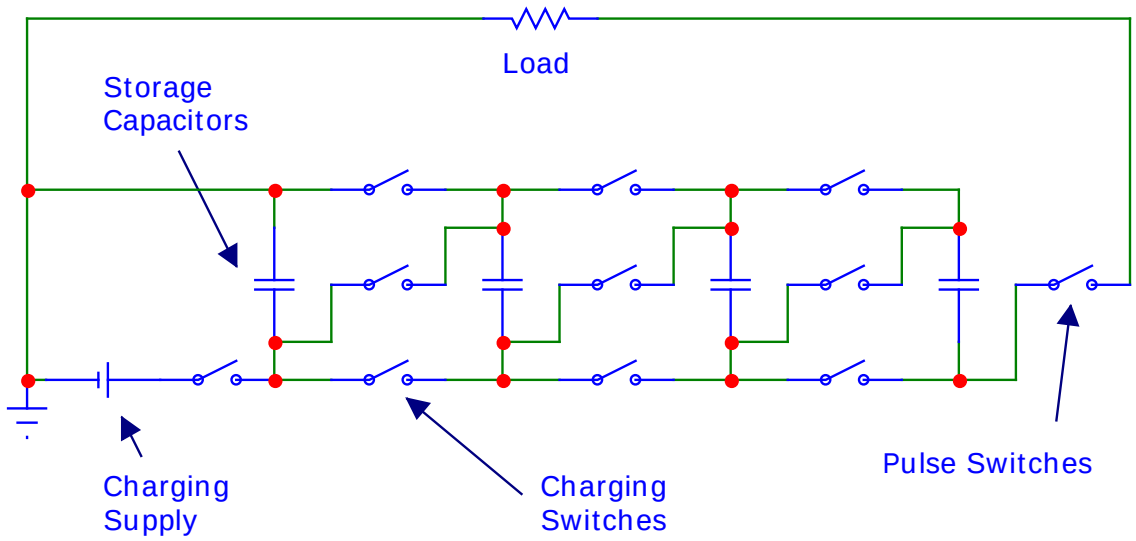

Figure 1.4: Switched Marx generator

Marx topologies utilizing solid state devices are commonly referred to as solid state Marx generators. For simplicity, and generality, the schematics below will continue to show generic switches rather than explicitly showing solid state MOSFETs or IGBTs.

Initially all switches are off as shown in Fig. 1.4. To charge the capacitors, the charging switches are turned on as shown in Fig. 1.5 and charge flows from the charging supply to the capacitors. When the capacitors are charged the charging switches are turned off.

When the output pulse is desired the pulse switches are turned on and current flows through the capacitors, which are now in series, and to the load as shown in Fig. 1.6. Unlike the spark gap Marx topologies, the solid state Marx allows the pulse to be cut off before the capacitors are fully discharged allowing for control of the pulse width. This also has the advantage over a non-Marx stacked switch topology (many switches in series connecting a load to a single capacitor bank) that each pulse switch only sees the charge voltage of its corresponding capacitor. However, during the output pulse the charging switches divide up the total output voltage; how this voltages is divided depends on the capacitance between each stage and that from each stage to ground. If the voltage is not evenly divided between the stages it is possible for a charging switch to have a voltage across it that is greater than it is rated for causing damage to the switch. To reduce cost, the charging switches

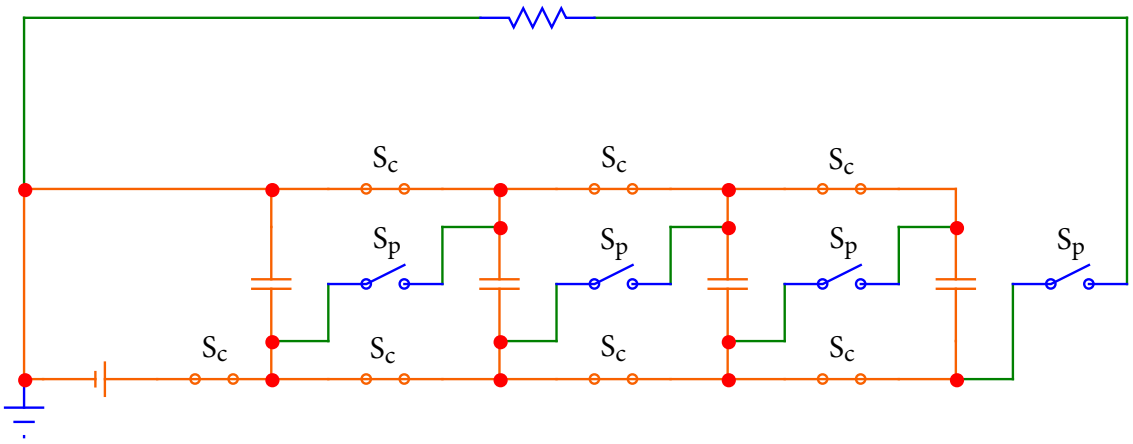

Figure 1.5: Switched Marx generator configured for charging capacitors in parallel. Charging switches, S_c, are closed and pulse switches, S_p, are open.

that will be reverse biased during the discharge portion of the cycle are commonly replaced with diodes as shown in Fig. 1.7. Additionally these diodes protect any pulse switches that turn on a little later than others from being damaged by a reverse voltage. This also gives the additional benefit of allowing the output voltage and pulse shape to be adjusted in increments of the stage voltage by turning some pulse switches on later or not at all [8].

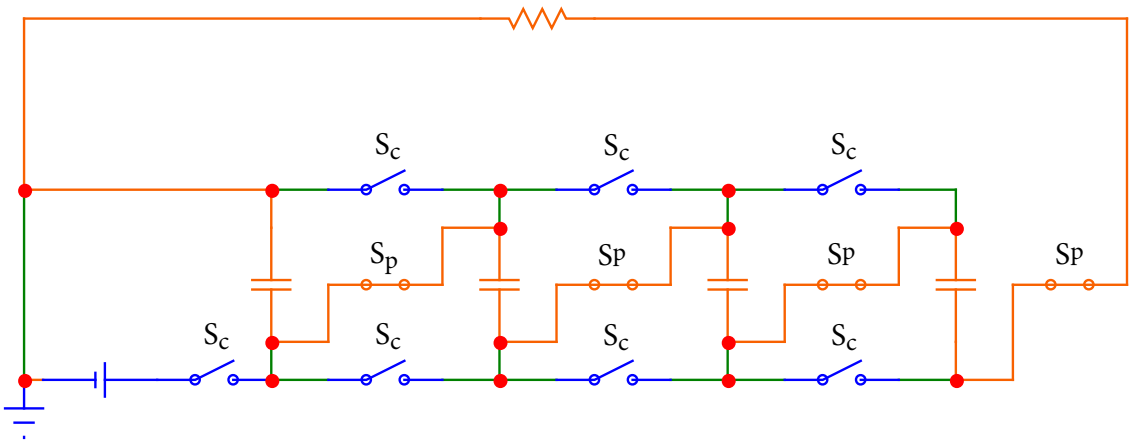

Figure 1.6: Switched Marx generator configured for discharging capacitors in series. Charging switches, S_c, are open and pulse switches, S_p, are closed.

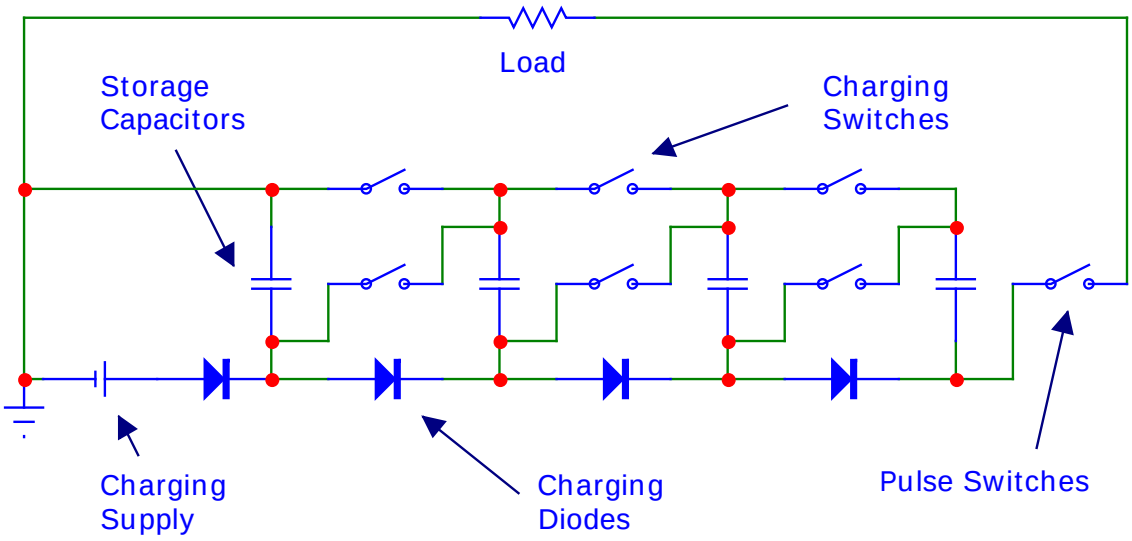

Figure 1.7: Switched Marx generator with charging diodes

The charging diodes and storage capacitors protect the pulse switches from seeing more voltage than intended but the remaining charging switches are vulnerable to over-voltage from transients at the beginning of the discharge portion of the cycle or during an arc. If stray capacitances are not carefully managed an individual charging switch could see more voltage than it is designed for causing permanent damage to the switch. Much of Marx generator research focuses on this issue. One possible solution is to eliminate the charging switches.

In 2002 R. Richter-Sand et al. described charging a Marx generator through a series of common mode chokes, similar to the circuit shown in Fig 1.8, to isolate the charging supply from the high voltage [9]. G. Lehy describes a similar topology in [10].

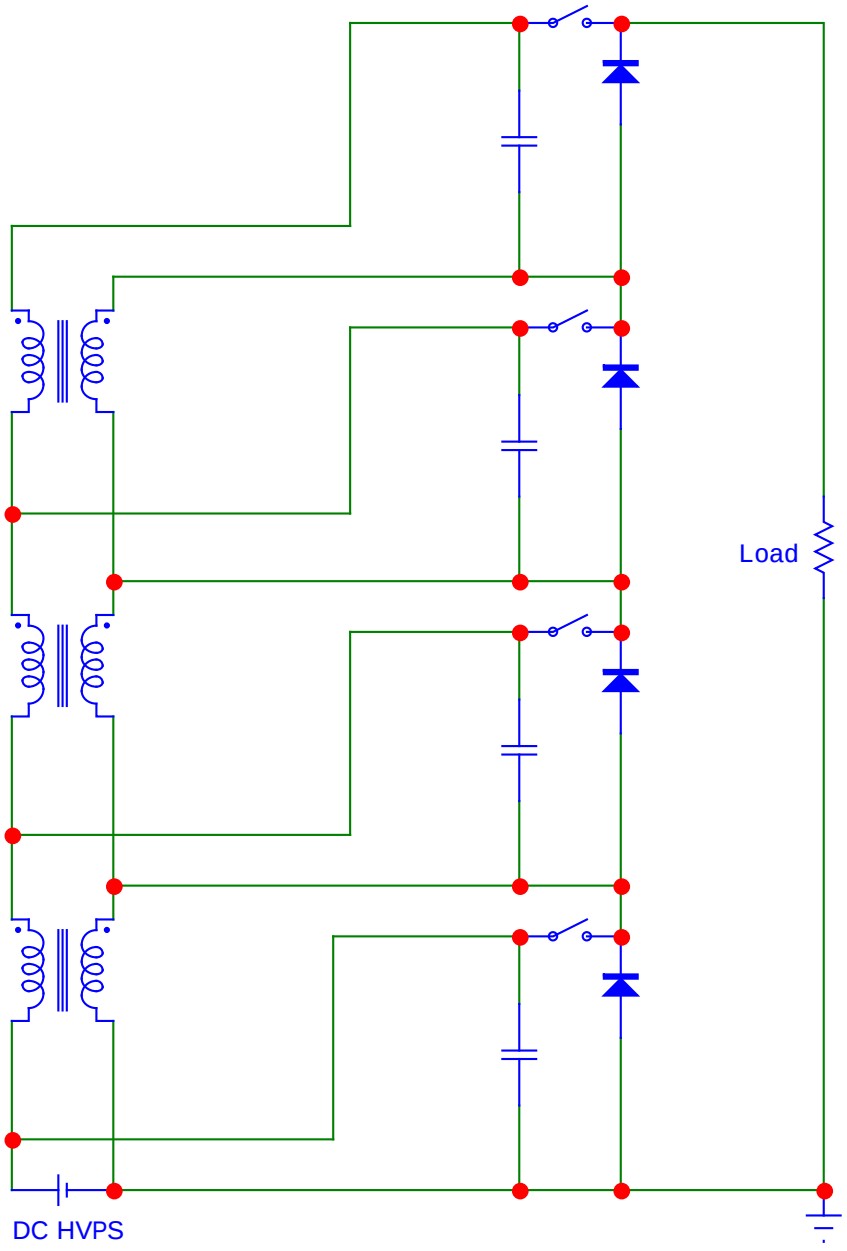

Figure 1.8: Marx generator charged through a series of common mode chokes

In 2006 H. Kirbie and G. Dale applied for patent describing a Marx generator similar to the circuit shown in Fig. 1.9 whereby the capacitors are charged through diodes and an

inductance in parallel with the load [11]. Similar circuits are discussed in [12] and [13].

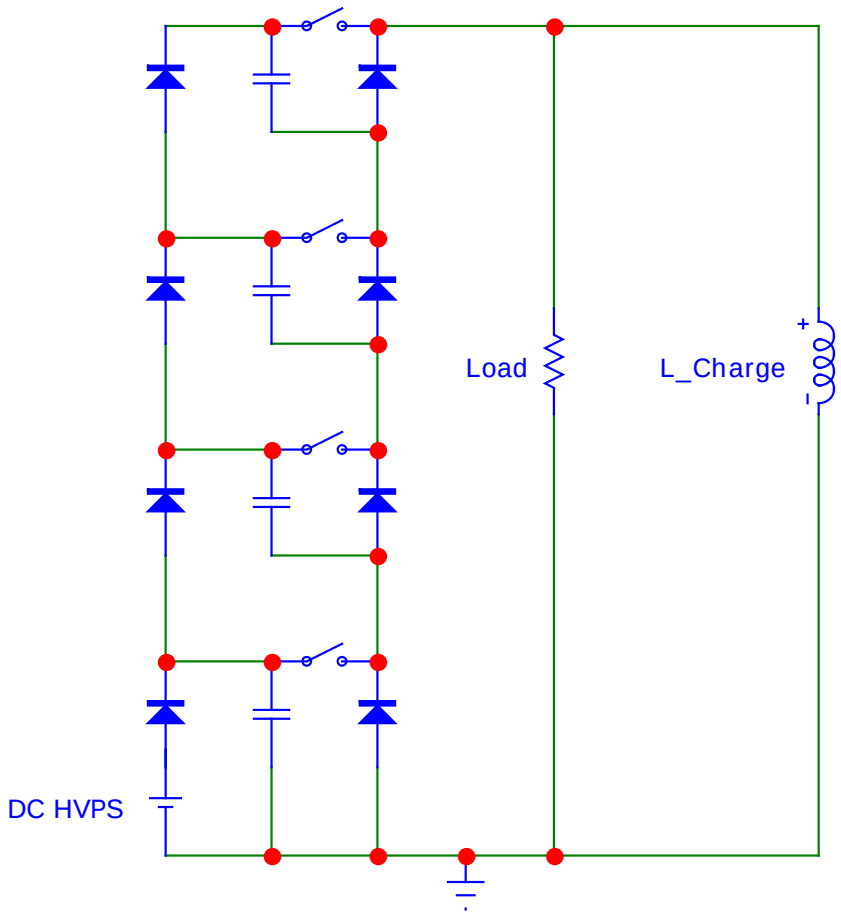

Figure 1.9: Marx generator charged through inductor in parallel with load

The Marx generator concept can be generalized to a system that charges multiple energy storage devices in parallel, or individually, and then connects them in series to increase the output voltage for discharge. We can think of a *generalized Marx generator* as a stack of circuits each of which contain energy storage and a switch. The challenge is to find a way to recharge the energy storage in a quick and reliable manner. This generalization is shown Fig. 1.10. As discussed previously, the diodes allow for any stage to remain off if desired and help protect the stages during turn off. The isolated power sources could be batteries or even gasoline powered generators but for practical long term use power must be coupled from something at or near ground potential. Transformers offer a robust way to

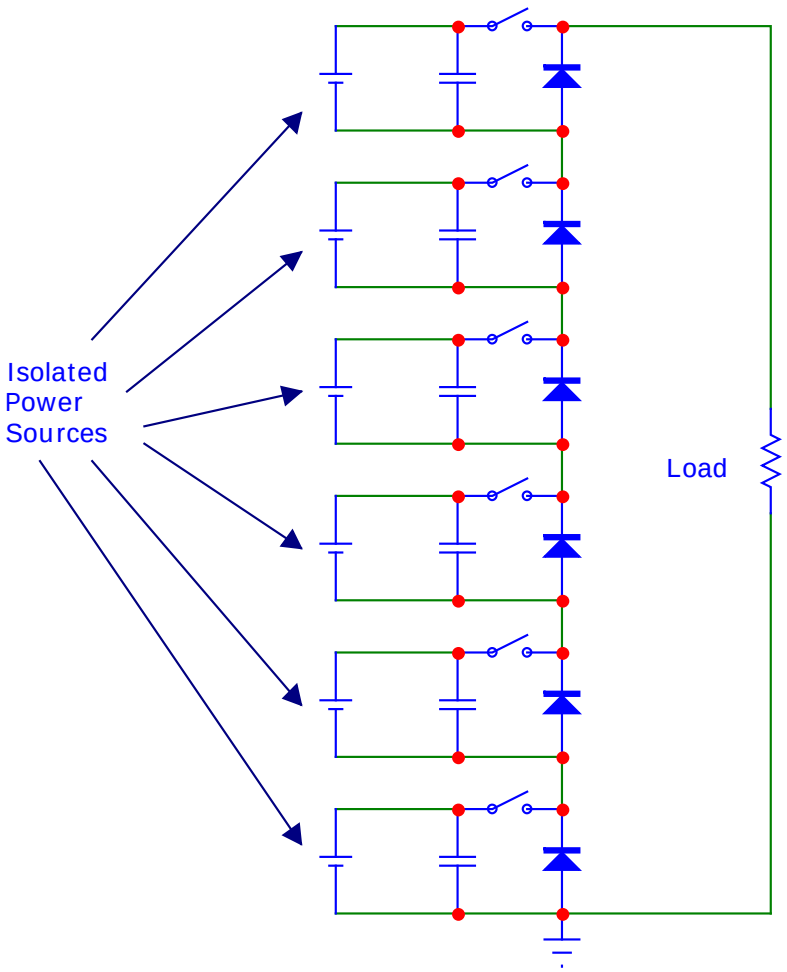

Figure 1.10: Generalized Marx generator

transfer power across high voltage isolation. Fig. 1.11 and Fig. 1.12 show Marx generators charged by isolation transformers. The circuit in Fig. 1.11 has been used successfully with large air core transformer (transformers that are magnetically coupled through free space rather than through a magnetic material) as described in [8]. This topology excels in several applications but the air core transformer must be large enough to achieve sufficient coupling while maintaining high voltage stand off and low primary to secondary parasitic capacitance. These circuits could, in principle, also be built with iron core transformers but they would still need to be large enough to hold off the high voltage and keep the primary to secondary capacitances down.

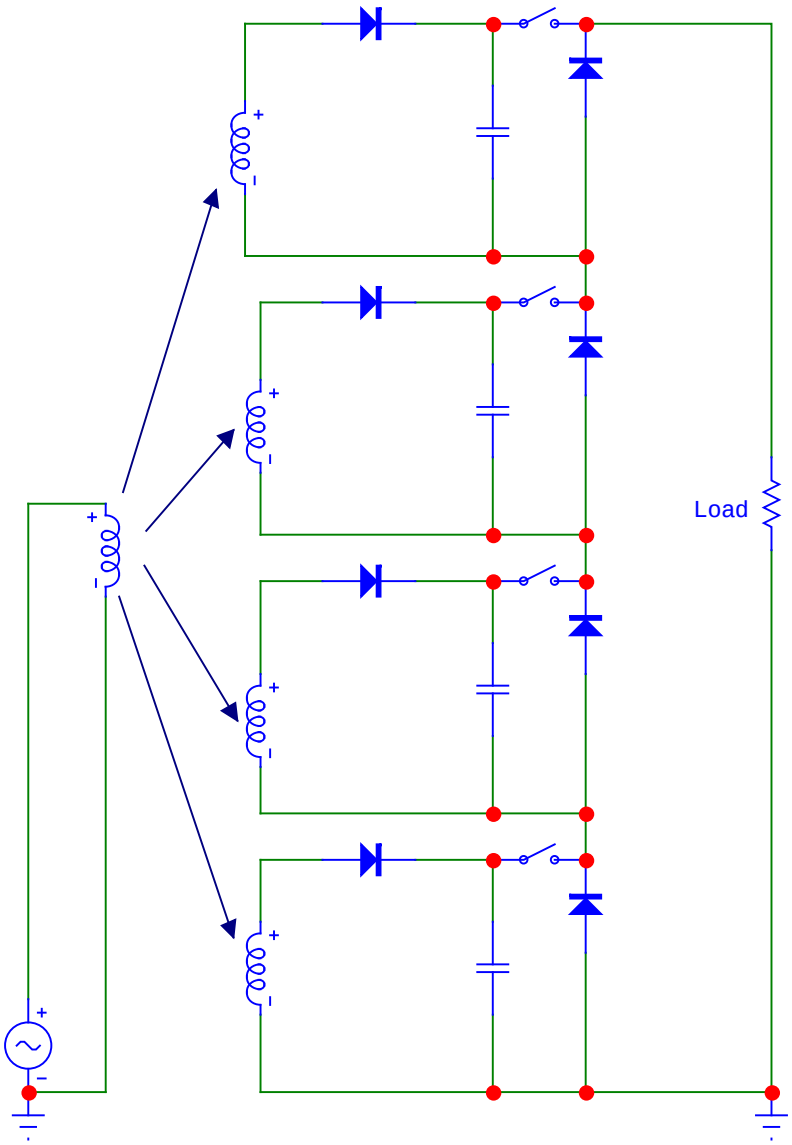

Figure 1.11: Marx generator charged via single isolation transformer with multiple secondary windings.

Another possible topology for charging the Marx stages are cascaded transformers shown in Fig. 1.13. The circuit topology shown in Fig. 1.13 can solve the issue with capacitance to ground but it creates another issue. With each stage of the cascaded transformer comes more source impedance. When scaled up to N stages, the Nth stage would see a source impedance that is at least N times higher than the first stage. The effect of this added impedance would be that the Nth stage would take at least N times longer to charge to the

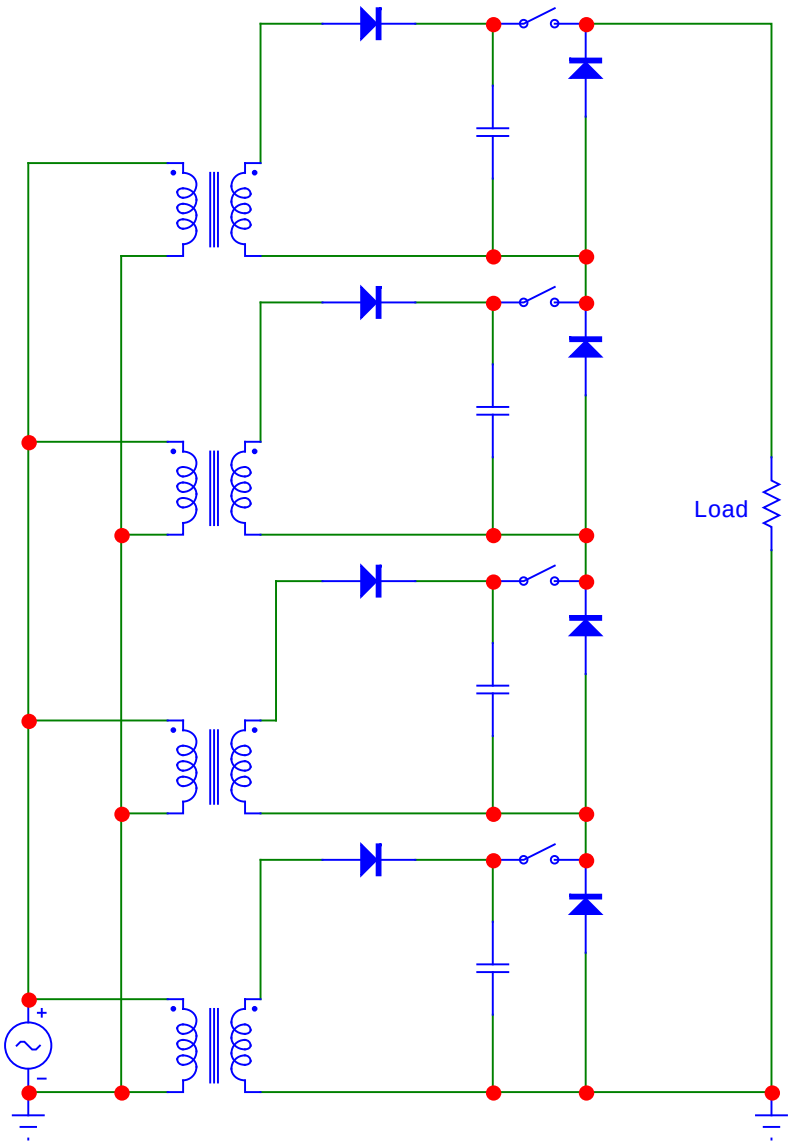

Figure 1.12: Marx generator charged via multiple isolation transformers.

same voltage as the first stage and each stage would see higher voltage droop under load than those before it. This could be corrected for a given load by adjusting the number of turns on the transformers to compensate for the decrease in voltage. However, this would still cause the voltage distribution between stages to change depending on the load.

If a capacitor is added to each stage of the cascaded transformers, as shown in Fig. 1.14, the cascaded transformers now becomes a system of N coupled oscillators, or cells, and can also be thought of as a discreet element transmission line. This configuration is

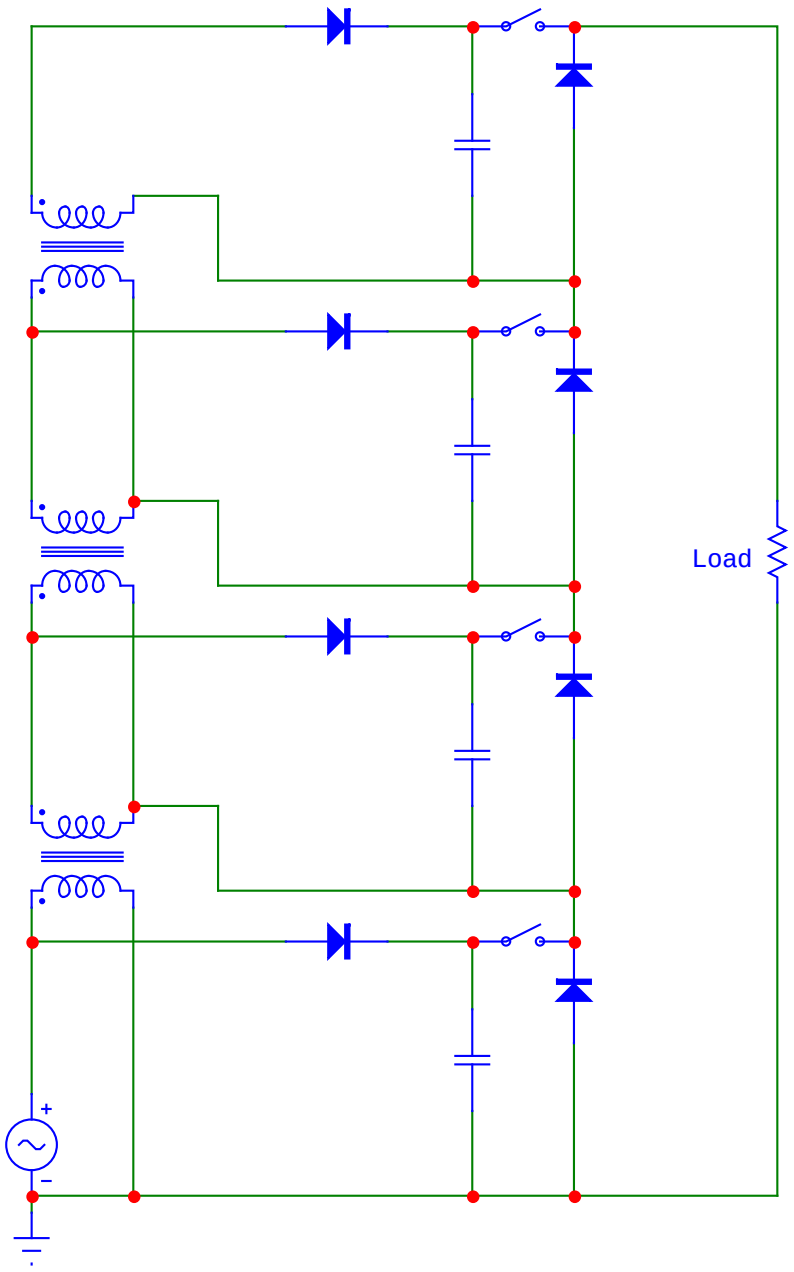

Figure 1.13: Marx Generator charged via cascaded transformers

mathematically equivalent to certain rf linear particle accelerators such as coupled cavity accelerators. [14] [15]. Some of the tools developed for the study of coupled cavity linear accelerators will be applied to this structure.

If the power losses are not too high, a system of N coupled oscillators will resonate at N different frequencies. At each of these frequencies, the system of oscillators will behave in

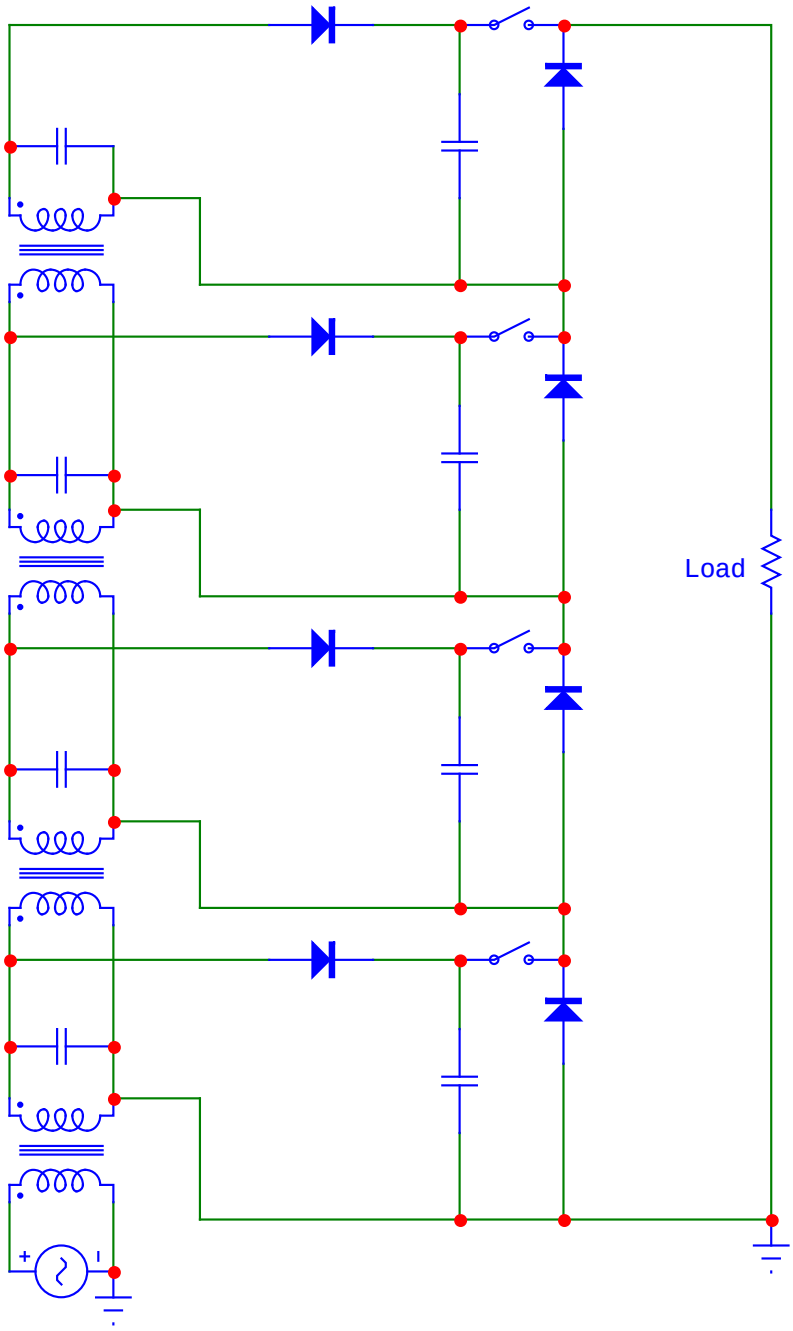

Figure 1.14: Marx generator charged via resonant cascaded transformers

a different way. The way in which the system behaves at a one of its resonant frequencies is often called the mode of oscillation, or simply mode. Each mode is characterized by the relative phases of the oscillations in the individual resonators. For example, if at some frequency all the individual resonators are in phase, the phase shift between resonators is

zero and this mode is referred to as the zero mode.

In an infinitely long lossless discrete element transmission line made of an infinite number of cells, or a finite system that is terminated appropriately, the magnitude of the oscillation in each cell is equal and only the phase differs. The infinite transmission line is not practical for our application due to parts cost and space requirements. The finite system driven on one end and terminated by a matched resistive load on the other, sometimes referred to as a traveling wave structure requires a large fraction of the input power to be dissipated into the termination resistance. If the structure is terminated into a an unmatched load, preferably an open or a short, the power that reached the end of the structure is reflected back up the structure toward the source. The sum of the forward traveling wave from the source and the backward traveling wave from the reflection add together to create a standing wave. Such a system is referred to as a standing wave structure. At steady state, after the structure is filled with energy and the standing wave is in place, the amplitude of oscillation is not necessarily equal at each cell and differs for each mode. The relative amplitudes of the cells at a given frequency is often refereed to as the spatial distribution.

In 1967 Enge filed a patent describing a traveling wave structure for the generation of high voltage composed of inductively coupled resonators but did not fully explore standing wave designs [16]. This traveling wave structure suffered from a large decrease in stage voltage for each successive stage unless a large amount of power was transferred through the structure with much of it being dissipated in the matched load at the end. A few years later in January of 1969 Enge filed a patent for an improvement to the previous invention that terminated the structure such that a standing wave was formed [17]. In one embodiment described, the capacitive termination was constantly varied to sweep the standing wave across the structure in order to allow each stage to charge to the same voltage. In another embodiment in the same patent, Enge described inductors being axially spaced such that

a third of the coils were at the axial field maxima and the reaming coils were placed to either side of the field maxima. The coils placed to either side of the field maxima were then connected in series to create the same voltage as the other coils. Later the same year, in July 1969, Enge submitted another patent which developed this idea further into a system of resonant cascaded transformers and added capacitive coupling between cells, however, it is not clear what mode this system was operated at [18].

If we were to charge a Marx generator with a standing wave structure operated in a arbitrarily chosen mode, and having the wrong spatial distribution, each stage of our Marx generator would charge to a different voltage resulting in an inefficient use of components. In order for each cell of our Marx generator to charge to the same voltage it is desirable that each resonator in the system oscillate with the same amplitude. For systems of two or more cells there are exactly two modes where all the amplitudes will be equal: the zero mode where all cells have equal amplitude and equal phase and the π mode where all cells have equal magnitude but opposite phase as their neighbors. We will show in the next chapter that these two modes each have their own difficulties in implementation. Meanwhile, there is another mode of interest that exists for finite structures made of an odd number of cells and that is the $\pi/2$ mode. In a finite structure operating in the $\pi/2$ mode every other cell has zero amplitude but the neighbors to these empty cells have equal magnitudes with opposite phases. We will show that there are some other useful properties of the $\pi/2$ that more than make up for approximately half, (N-1)/2, of the resonators being "empty". The cells with zero amplitude, commonly referred to as coupling cells, will not contribute to the output and so there is no need to attach rectifiers or switches to them in our application. In fact we also have the freedom to change the characteristic impedance of the coupling cells resulting in a biperiodic structure. Removing the rectifiers and switches from the coupling cells, but leaving them on the active cells gives us the circuit shown in Fig. 1.15. We will study this

circuit in the upcoming chapters.

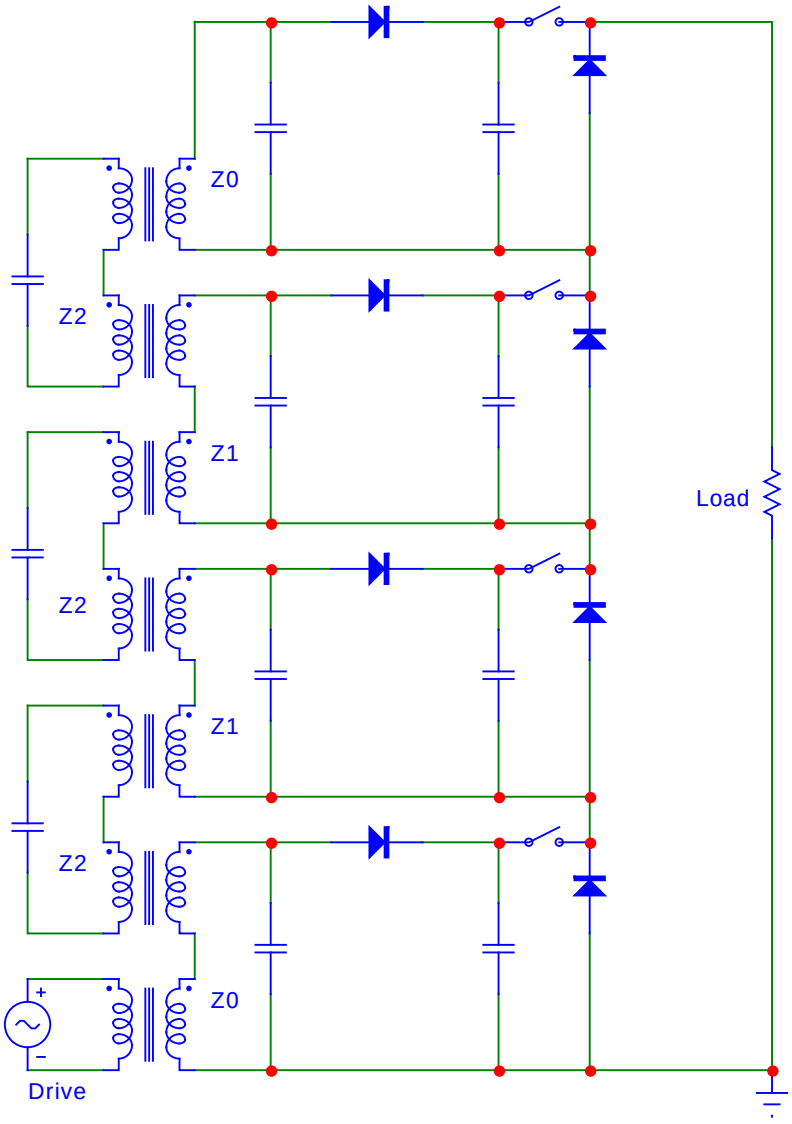

Figure 1.15: Marx generator charged via biperiodic resonant cascaded transformers

CHAPTER 2

$\pi/2$ MODE

As discussed earlier, a system composed of N coupled oscillators will have N unique modes of oscillation. Each mode is characterized by the phase shift between neighboring cells. For systems with inductive coupling, the lowest frequency is the one in which all cells are in phase (zero phase shift) and is referred to as the "zero mode". The highest frequency mode for inductively coupled systems is the one in which each cell is 180 degrees out of phase with its neighbors (phase shift of π radians) and is referred to as the "π mode". Systems with odd numbers of cells have a $\pi/2$ mode (pronounced either "pi-over-two" or "pi halves") which is the middle mode sequentially though its frequency is not necessarily half way between the zero and π mode. The relationship of a mode's phase shift between cells and the mode's frequency is described by the system's *dispersion equation* and its graphical representation is known as a *dispersion diagram*. [19] [20] For finite systems, the resonant frequencies can be calculated analytically by solving the eigensystem corresponding to the system's Kirchhoff circuit equations. This will be demonstrated in Chapter 3.

Although we will be dealing with a finite system of oscillators for our modulator, it is useful to take a moment and consider the case of infinite oscillators with infinite modes. If we remove the rectifiers, energy storage capacitors, pulse switches, and other modulator related circuitry from the circuit in Fig. 1.15 we are left with only the oscillators themselves

as shown in Fig. 2.1.

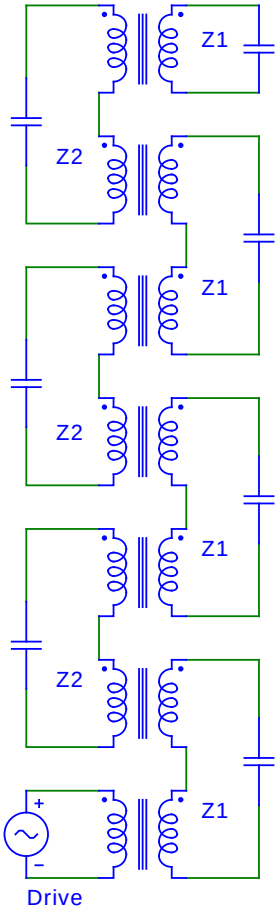

Figure 2.1: Chain of biperiodic coupled oscillators

For a biperiodic system, this can be simplified to just the two resonator circuits shown in Fig. 2.2 with equivalent circuit shown in Fig. 2.3.

The Kirchhoff circuit equations for the system in Fig. 2.3 can be expressed as

$$\begin{aligned} 0 &= -\mathcal{I}_{2n}\left(2j\omega\mathcal{L}_2 + \tfrac{1}{j\omega\mathcal{C}_2}\right) + \mathcal{I}_{2n-1}j\omega\mathcal{M}_{12} + \mathcal{I}_{2n+1}j\omega\mathcal{M}_{12} \\ 0 &= -\mathcal{I}_{2n+1}\left(2j\omega\mathcal{L}_1 + \tfrac{1}{j\omega\mathcal{C}_1}\right) + \mathcal{I}_{2n}j\omega\mathcal{M}_{12} + \mathcal{I}_{2n+2}j\omega\mathcal{M}_{12}, \end{aligned} \tag{2.1}$$

where $\mathcal{M}_{12}$ is defined by

$$\mathcal{M}_{12} = k\sqrt{\mathcal{L}_1\mathcal{L}_2}. \tag{2.2}$$

Suppose the currents in each loop of the circuit vary with time as cosine functions such

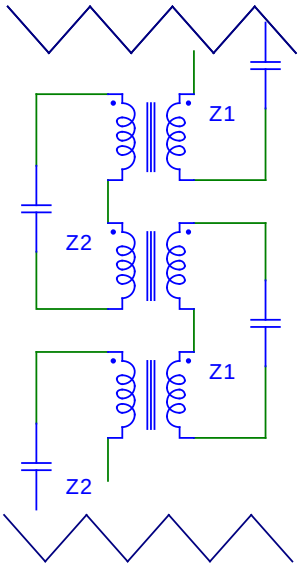

Figure 2.2: One unit of an infinite chain of biperiodic oscillators

that

$$\begin{aligned}
\mathcal{I}_{2n-1} &= \mathbb{I}_{\text{odd}} Re\left[e^{i(\phi+\omega t)}\right] \\
\mathcal{I}_{2n} &= \mathbb{I}_{\text{even}} Re\left[e^{i\omega t}\right] \\
\mathcal{I}_{2n+1} &= \mathbb{I}_{\text{odd}} Re\left[e^{i(\omega t-\phi)}\right] \\
\mathcal{I}_{2n+2} &= \mathbb{I}_{\text{even}} Re\left[e^{i(\omega t-2\phi)}\right]
\end{aligned} \tag{2.3}$$

and

$$\begin{aligned}
\omega_1 &= \tfrac{1}{\sqrt{2\mathcal{C}_1\mathcal{L}_1}} \\
\omega_2 &= \tfrac{1}{\sqrt{2\mathcal{C}_2\mathcal{L}_2}}.
\end{aligned} \tag{2.4}$$

Substituting Eqs. 2.2, 2.3, and 2.4 into Eq. 2.1 and solving for ω in terms of ϕ yields

$$\omega(\phi) = \sqrt{-\frac{\omega_1^2+\omega_2^2 \pm \sqrt{4k^2\omega_1^2\omega_2^2\cos^2(\phi) + \left(\omega_1^2-\omega_2^2\right)^2}}{k^2\cos(2\phi)+k^2-2}}. \tag{2.5}$$

This function represents two pass bands with each pass band determined by the sign in front of the inner square root. For illustration, Fig. 2.4 depicts these curves for $k = 0.9$, $\omega_1 = 0.9\omega_0$, and $\omega_2 = 1.1\omega_0$, with ω_0 a reference angular frequency.

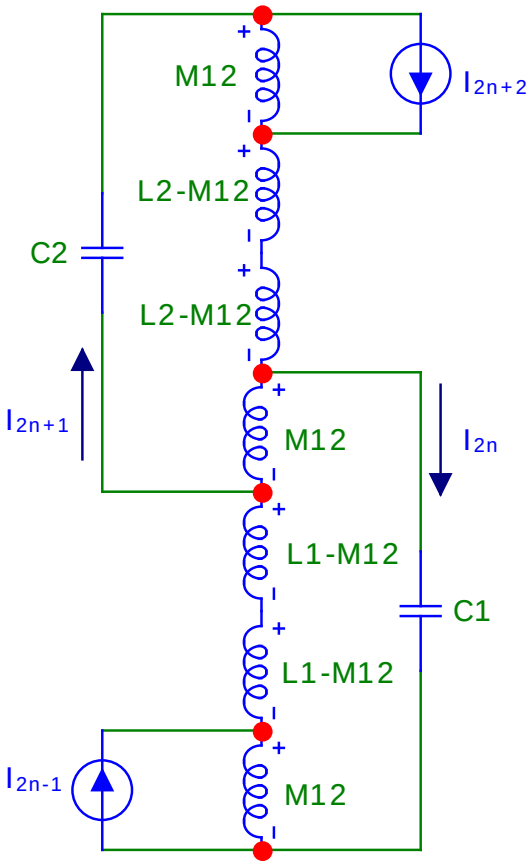

Figure 2.3: Equivalent circuit for infinite chain of biperiodic oscillators

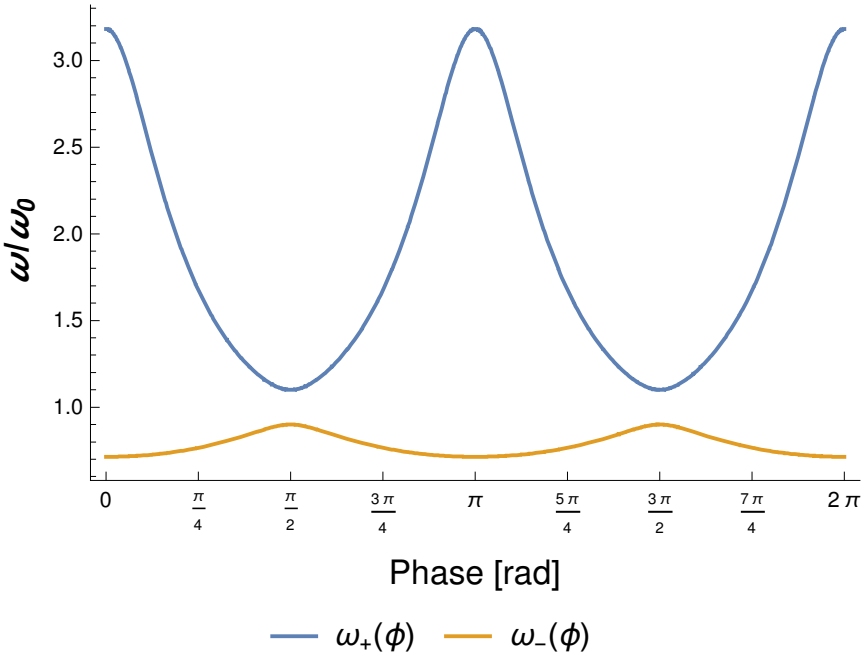

Figure 2.4: Dispersion plot for an illustrative example

For forward traveling waves, the group velocity will be positive and therefore the slope of the dispersion curve will be positive [20]. Limiting each of these curves to the domain where their slope is positive gives the curves shown in figure Fig. 2.5. The frequency range between the two curves is the *stopband*.

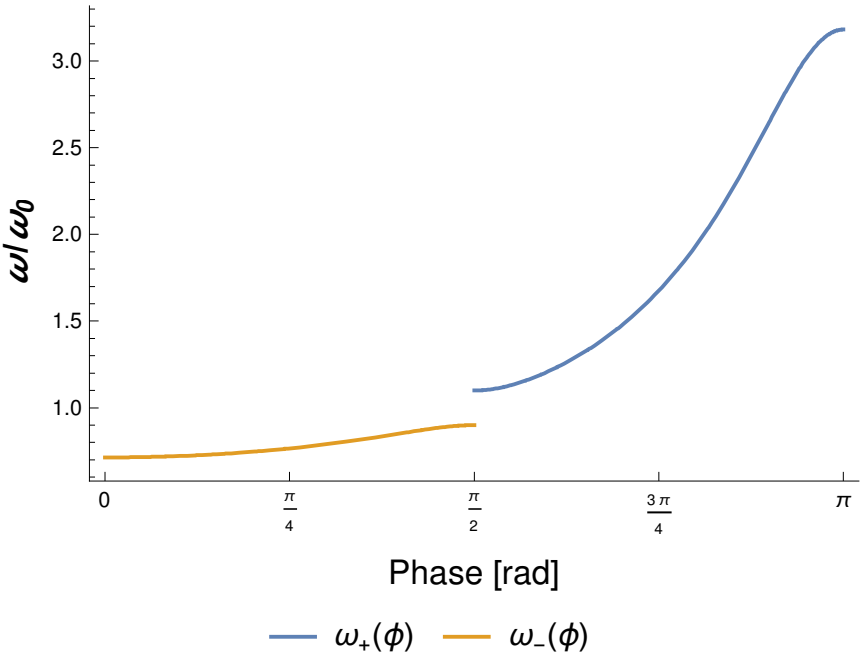

Figure 2.5: Dispersion plot for forward traveling waves

When ω_1 and ω_2 are equal to ω_0, Eq. 2.5 simplifies to

$$\omega(\phi) = \sqrt{-\frac{2\omega_0^2 - 2 \pm \sqrt{k^2\omega_0^4\cos^2(\phi)}}{k^2\cos(2\phi) + k^2 - 2}} \tag{2.6}$$

and the stopband closes as shown in Fig. 2.6. When the stopband is closed, the discontinuity in the dispersion equation at $\phi = \pi/2$ is removed with the function taking the value $\omega(\pi/2) = \omega_0$ independent of the coupling constant, k. This lack of dependence on the coupling when the phase shift equals $\pi/2$ is one of the advantages of using the $\pi/2$ mode.

A further advantage of the $\pi/2$ mode over the zero and π modes can also be seen from examination of the dispersion curve. Taking the derivative of Eq. 2.6 it can be shown that

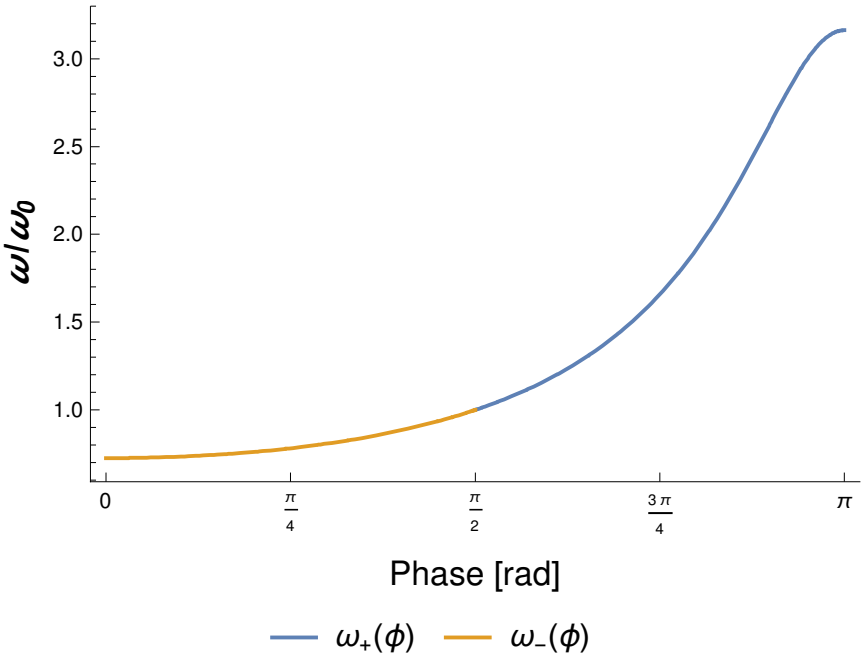

Figure 2.6: Dispersion plot with stopband closed

the group velocity is zero when the phase shift is zero or π, but is equal to $k\omega_0/2$ when the phase shift is $\pi/2$. It is desirable that the slope of the dispersion curve not be zero at our operating point for two reasons. The slope of the dispersion curve is related to the frequency spacing between adjacent modes and where the dispersion curve is flat, modes are more closely spaced. The second reason is that, as stated earlier, the group velocity is equal to slope of the dispersion curve and waves with zero group velocity do not propagate energy down the structure efficiently.

A structure operating in the zero mode was shown to create a fairly flat voltage distribution in [21] and its utility for charging a Marx generator was discussed in [22]. This resonant system relied on strong Nth neighbor coupling. Coupling between inductors falls off with distance but, due to the design of the indictors, nearest neighbour coupling was about 70%, next nearest neighbor coupling was about 50% and the coupling did not fall below 10% until the eighth or ninth neighbors. Maintaining large coupling to multiple inductors without sacrificing high voltage stand off required large flat air-core inductors that were about ten times

larger in diameter then the spacing between cells. The long range coupling likely helped the power propagate down the structure. It is not clear how well this structure would scale for designs where the length of the structure was much longer than the diameter of the coils.

As stated in Chapter 1, it is desirable that all of the resonators have approximately equal voltage so that the maximum output voltage is achieved for the chosen components. Keeping the voltages of each resonator approximately equal is desirable because the output voltage of the Marx generator will be the average stage voltage multiplied by the number of stages, but the devices in each stage must be rated for the maximum voltage of any stage if we wish to use the same devices for each stage. If all the stages operate at the same voltage, then the average voltage of all stages is equal to the maximum voltage of any stage and the devices will be used efficiently. The only modes where the amplitudes of the oscillator in a finite structure are equal are the zero mode and the π modes. However both of these modes have zero group velocity and a dependence on the coupling value. The $\pi/2$ mode in a finite systems on the other hand has equal amplitudes albeit in every other cell. Additionally, the $\pi/2$ frequency is not dependent on the coupling between cells and has a non zero group velocity when the bandgap is closed. We choose to operate this Marx generator charging system, shown in Fig. 1.15, in the $\pi/2$ mode because of these advantages over other modes.

CHAPTER 3

COUPLED OSCILLATOR CIRCUIT MATRIX EQUATION

For a system of coupled resonators containing a finite number of cells, the modes of the system can be calculated using matrix analysis. We will start by reducing the circuit in Fig. 2.1 to a more simplified form shown in Fig. 3.1.

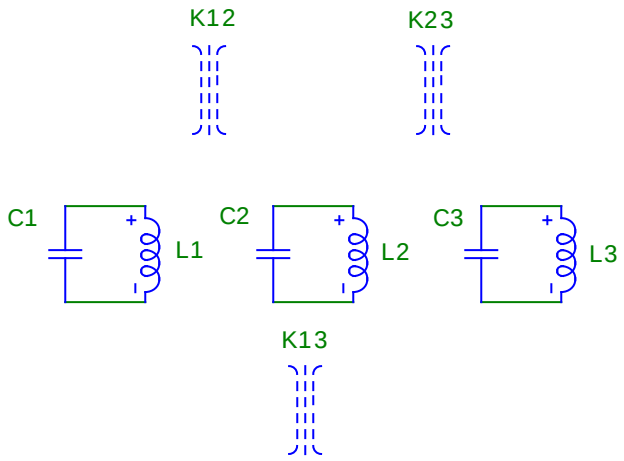

Figure 3.1: Three coupled LC oscillators

Using Kirchhoff's voltage law, we can write an equation for each current loop such that

the sum of voltages around each loop is equal to zero as shown in Eq. 3.1

$$\begin{aligned} 0 &= \mathcal{I}_1 j\omega\mathcal{L}_1 + j\omega\mathcal{I}_2\mathcal{M}_{12} + j\omega\mathcal{I}_3\mathcal{M}_{13} + \mathcal{V}_{\mathcal{C}1} \\ 0 &= \mathcal{I}_2 j\omega\mathcal{L}_2 + j\omega\mathcal{I}_1\mathcal{M}_{21} + j\omega\mathcal{I}_3\mathcal{M}_{23} + \mathcal{V}_{\mathcal{C}2} \\ 0 &= \mathcal{I}_3 j\omega\mathcal{L}_3 + j\omega\mathcal{I}_1\mathcal{M}_{31} + j\omega\mathcal{I}_2\mathcal{M}_{32} + \mathcal{V}_{\mathcal{C}3} \end{aligned} \tag{3.1}$$

where the mutual inductance, $\mathcal{M}$, of inductors m and n is given by [23]

$$\mathcal{M}_{\mathrm{mn}} = \mathcal{M}_{\mathrm{nm}} = \mathcal{K}_{\mathrm{mn}}\sqrt{\mathcal{L}_m\mathcal{L}_n}. \tag{3.2}$$

To get the equations in terms of voltage only, we replace each $\mathcal{I}_n$ with the current through the capacitor $\mathcal{C}_n$ using the generalized form of Ohm's law, $\mathcal{I}_n = \mathcal{V}_{\mathcal{C}n}/Z_{\mathcal{C}n}$, and the capacitor's impedance, $\mathcal{Z}_{\mathcal{C}n} = 1/(j\omega\mathcal{C}_n)$.

$$\begin{aligned} 0 &= -\mathcal{V}_{\mathcal{C}1}\mathcal{C}_1\mathcal{L}_1\omega^2 - \mathcal{V}_{\mathcal{C}2}\mathcal{C}_2\mathcal{M}_{12}\omega^2 - \mathcal{V}_{\mathcal{C}3}\mathcal{C}_3\mathcal{M}_{13}\omega^2 + \mathcal{V}_{\mathcal{C}1} \\ 0 &= -\mathcal{V}_{\mathcal{C}2}\mathcal{C}_2\mathcal{L}_2\omega^2 - \mathcal{V}_{\mathcal{C}1}\mathcal{C}_1\mathcal{M}_{21}\omega^2 - \mathcal{V}_{\mathcal{C}3}\mathcal{C}_3\mathcal{M}_{23}\omega^2 + \mathcal{V}_{\mathcal{C}2} \\ 0 &= -\mathcal{V}_{\mathcal{C}3}\mathcal{C}_3\mathcal{L}_3\omega^2 - \mathcal{V}_{\mathcal{C}1}\mathcal{C}_1\mathcal{M}_{31}\omega^2 - \mathcal{V}_{\mathcal{C}2}\mathcal{C}_2\mathcal{M}_{32}\omega^2 + \mathcal{V}_{\mathcal{C}3} \end{aligned} \tag{3.3}$$

We gather the ω terms by dividing by $-\omega^2$ to arrive at

$$\begin{aligned} 0 &= \mathcal{C}_1\mathcal{L}_1\mathcal{V}_{\mathcal{C}1} - \tfrac{\mathcal{V}_{\mathcal{C}1}}{\omega^2} + \mathcal{C}_2\mathcal{M}_{12}\mathcal{V}_{\mathcal{C}2} + \mathcal{C}_3\mathcal{M}_{13}\mathcal{V}_{\mathcal{C}3} \\ 0 &= \mathcal{C}_1\mathcal{M}_{21}\mathcal{V}_{\mathcal{C}1} + \mathcal{C}_2\mathcal{L}_2\mathcal{V}_{\mathcal{C}2} - \tfrac{\mathcal{V}_{\mathcal{C}2}}{\omega^2} + \mathcal{C}_3\mathcal{M}_{23}\mathcal{V}_{\mathcal{C}3} \\ 0 &= \mathcal{C}_1\mathcal{M}_{31}\mathcal{V}_{\mathcal{C}1} + \mathcal{C}_2\mathcal{M}_{32}\mathcal{V}_{\mathcal{C}2} + \mathcal{C}_3\mathcal{L}_3\mathcal{V}_{\mathcal{C}3} - \tfrac{\mathcal{V}_{\mathcal{C}3}}{\omega^2} \end{aligned} \tag{3.4}$$

We want this in matrix form so we factor out the vector $\vec{\mathcal{V}}$ which results in

$$0 = \begin{pmatrix} \mathcal{C}_1\mathcal{L}_1 - \frac{1}{\omega^2} & \mathcal{C}_2\mathcal{M}_{12} & \mathcal{C}_3\mathcal{M}_{13} \\ \mathcal{C}_1\mathcal{M}_{21} & \mathcal{C}_2\mathcal{L}_2 - \frac{1}{\omega^2} & \mathcal{C}_3\mathcal{M}_{23} \\ \mathcal{C}_1\mathcal{M}_{31} & \mathcal{C}_2\mathcal{M}_{32} & \mathcal{C}_3\mathcal{L}_3 - \frac{1}{\omega^2} \end{pmatrix} \begin{pmatrix} \mathcal{V}_{\mathcal{C}1} \\ \mathcal{V}_{\mathcal{C}2} \\ \mathcal{V}_{\mathcal{C}3} \end{pmatrix} \tag{3.5}$$

Factoring out the different terms in the matrix gives

$$0 = \left(\begin{pmatrix} \mathcal{L}_1 & \mathcal{M}_{12} & \mathcal{M}_{13} \\ \mathcal{M}_{21} & \mathcal{L}_2 & \mathcal{M}_{23} \\ \mathcal{M}_{31} & \mathcal{M}_{32} & \mathcal{L}_3 \end{pmatrix} \begin{pmatrix} \mathcal{C}_1 & 0 & 0 \\ 0 & \mathcal{C}_2 & 0 \\ 0 & 0 & \mathcal{C}_3 \end{pmatrix} - \begin{pmatrix} \frac{1}{\omega^2} & 0 & 0 \\ 0 & \frac{1}{\omega^2} & 0 \\ 0 & 0 & \frac{1}{\omega^2} \end{pmatrix} \right) \begin{pmatrix} \mathcal{V}_{\mathcal{C}1} \\ \mathcal{V}_{\mathcal{C}2} \\ \mathcal{V}_{\mathcal{C}3} \end{pmatrix} \tag{3.6}$$

We can write this matrix equation more compactly, and more generally as

$$0 = \left(\mathcal{M}\mathcal{C} - \frac{\mathbb{I}}{\omega^2} \right) \vec{\mathcal{V}} \tag{3.7}$$

which we recognize as an eigenvector equation with eigenvector $\vec{\mathcal{V}}$, eigenvalues $\frac{1}{\omega^2}$, and matrix $\mathcal{M}\mathcal{C}$. Using Eq. 3.2 we can express $\mathcal{M}$ in terms of individual inductor values and couplings.

$$\mathcal{M} = \begin{pmatrix} \mathcal{L}_1 & k_{12}\sqrt{\mathcal{L}_1\mathcal{L}_2} & k_{13}\sqrt{\mathcal{L}_1\mathcal{L}_3} \\ k_{21}\sqrt{\mathcal{L}_2\mathcal{L}_1} & \mathcal{L}_2 & k_{23}\sqrt{\mathcal{L}_2\mathcal{L}_3} \\ k_{31}\sqrt{\mathcal{L}_3\mathcal{L}_1} & k_{32}\sqrt{\mathcal{L}_3\mathcal{L}_2} & \mathcal{L}_3 \end{pmatrix} \tag{3.8}$$

Using the Hadamard product, $\circ$, where $(\mathcal{A} \circ \mathcal{B})_{\mathrm{mn}} = \mathcal{A}_{\mathrm{mn}}\mathcal{B}_{\mathrm{mn}}$ we can separate the coupling and inductance terms.

$$\mathcal{M} = \begin{pmatrix} 1 & k_{12} & k_{13} \\ k_{21} & 1 & k_{23} \\ k_{31} & k_{32} & 1 \end{pmatrix} \circ \begin{pmatrix} \mathcal{L}_1 & \sqrt{\mathcal{L}_1\mathcal{L}_2} & \sqrt{\mathcal{L}_1\mathcal{L}_3} \\ \sqrt{\mathcal{L}_2\mathcal{L}_1} & \mathcal{L}_2 & \sqrt{\mathcal{L}_2\mathcal{L}_3} \\ \sqrt{\mathcal{L}_3\mathcal{L}_1} & \sqrt{\mathcal{L}_3\mathcal{L}_2} & \mathcal{L}_3 \end{pmatrix} \tag{3.9}$$

This can be written more generally and compactly as

$$\mathcal{M} = \mathcal{K} \circ \sqrt{\mathcal{L}\mathcal{L}^{\mathsf{T}}}, \tag{3.10}$$

where $\mathcal{L}$ is a single column matrix made of the inductor values. Lastly, using Eq. 3.10 for

the mutual inductance matrix, $\mathcal{M}$, in Eq. 3.7 gives

$$0 = \left(\left(\mathcal{K} \circ \sqrt{\mathcal{L}\mathcal{L}^{\mathsf{T}}} \right) \mathcal{C} - \frac{\mathbb{I}}{\omega^2} \right) \vec{\mathcal{V}} \tag{3.11}$$

One can take advantage of Eq. 3.11 by populating it with the appropriate inductance, capacitance, and coupling values and solving for the eigenvalues and eigenvectors. Each of the eigenvalues of Eq. 3.11 corresponds to a resonant mode of the system with the eigenvalue equal to $\frac{1}{\omega^2}$ where ω is the undriven, unloaded angular frequency of that mode. The eigenvectors of Eq. 3.11 correspond to the voltage distribution of the capacitors for each mode also known as *spatial distribution*. The magnitude of the n^{th} element of a mode's eigenvector is the amplitude of the voltage across the n^{th} capacitor when the system is operating at that mode. Eq. 3.11 can also be use "in reverse" to calculate capacitor or inductor values for a chosen spatial distribution at a specific frequency though care must be taken not to over determine or undetermine the system when doing so [24]. Additionally, the above derivation can be repeated for a circuit with losses by adding resistors in parallel to the capacitors. These resistances can be carried through in the derivation as a imaginary term in the capacitor matrix. Such a derivation is useful for studying the driven equivalent circuit with losses but will be left for future work. Chapter 4 discuses the construction of a bench top physical model and compares the measured mode frequencies to those calculated using 3.11 and to those measured in a SPICE simulated model in the frequency domain.

CHAPTER 4

MODEL, SPICE SIMULATION, AND MATRIX ANALYSIS

4.1 SIMPLE PHYSICAL BENCH MODEL

To confirm the work of Chapters 2 and 3, I built a small, low power, bench top model of the resonant circuit in Fig. 2.1. Low voltage, low loss capacitors are easy enough to acquire but the transformers required a suitable low loss core. I employed small cores, Fair-Rite PN 5978008001, left over from a previous project. One turn around this core was measured to have an inductance of 7.6 μH. Ten turns around this core were measured to have an inductance of 766 μH. Both measurements were made at 10 kHz using an Agilent (now Keysight) E4990A impedance analyzer. Next I designed a resonator where the coupling cells have one turn around each core and the active cells have ten turns around each core. I selected a $\pi/2$ mode frequency around 100 kHz. From Figure 2.1 we can see that the total inductance in each current loop is the sum of the inductance from each transformer winding in that circuit. Using equations 2.4 and the design frequency of 100 kHz, the capacitance needed for the active cells was 1.6 nF and the capacitance needed for the coupling cells was 160 nF. Using available 330 nF polypropylene capacitors for the coupling cells, and

available 3 nF and 0.36 nFp mica capacitors in parallel for the active cells lowered the $\pi/2$ mode frequency to about 70 kHz which was still a reasonable value for the cores. A five cell resonator was built consisting of three active cells and two coupling cells. The active cells were made by wrapping ten turns of RG-174/U coax around two cores combined with 3.0 nF and 0.36 nF capacitors in parallel. The center conductor and braid on each end of the of the coax were soldered together before being soldered to each side of the capacitors. The straightened length of RG-174/U for each inductor was about 825 mm. One of the active cell transformers is shown is shown in Fig. 4.1.

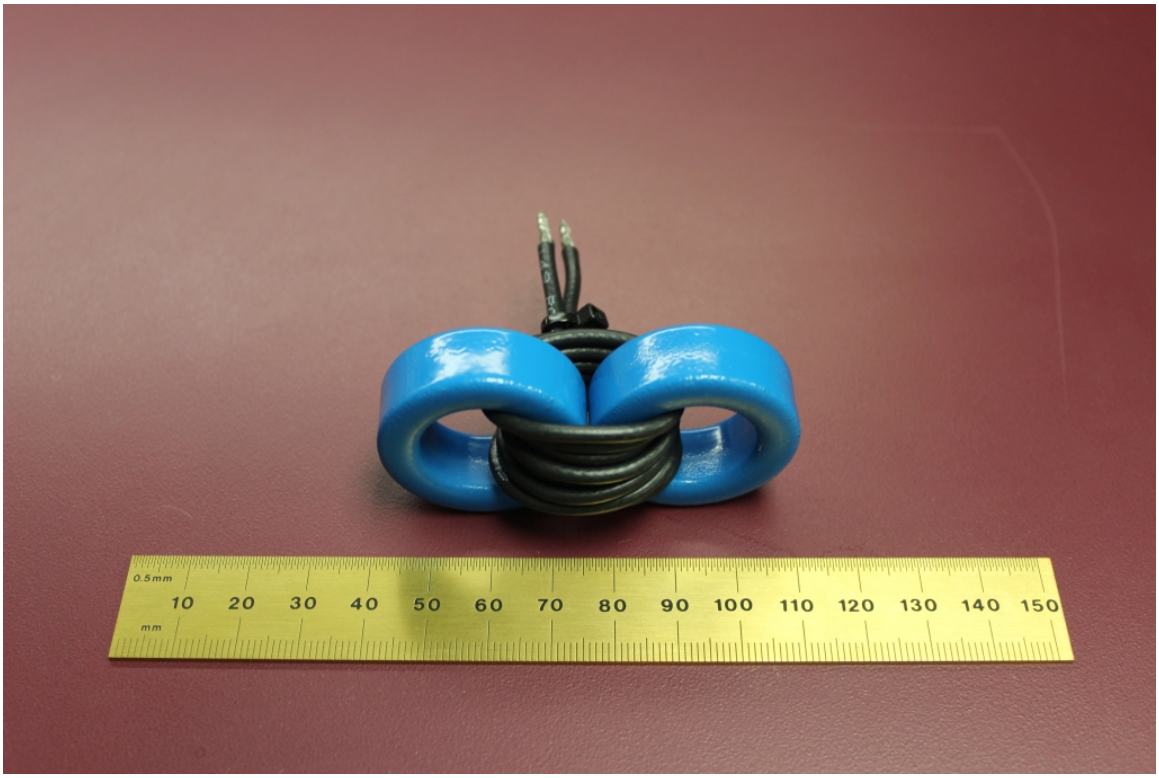

Figure 4.1: Two active cell inductors in series

The coupling cells were made by placing insulating sleeving on the terminals of a 330 nF polypropylene capacitor and running the terminals each through the appropriate core before soldering them together. A photograph of the complete resonator system in shown Fig. 4.2

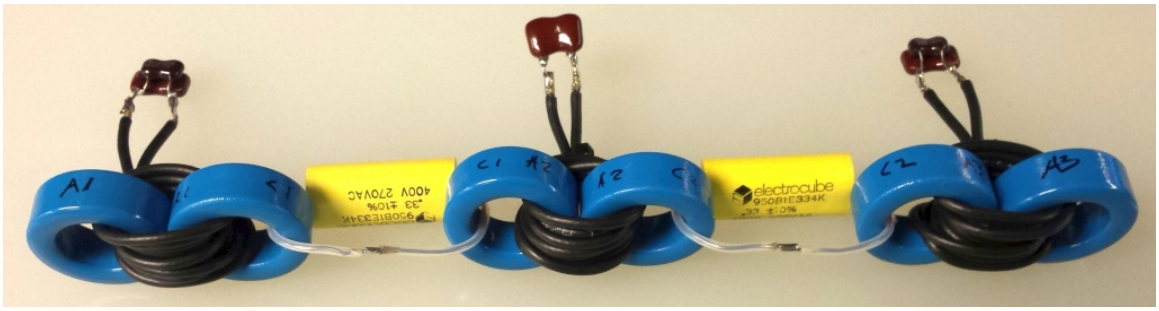

Figure 4.2: Five cell biperiodic resonant system

Individual component electrical properties, inductance, capacitance, and equivalent series resistance (ESR), were measured with the impedance analyzer at 75 kHz and are shown in Table 4.1.

Table 4.1: Electrical properties of components used to build five cell system as measured at 75 kHz

Cell	Inductance [mH]	Inductor ESR [Ω]	Capacitance [nF]	Capacitor ESR [mΩ]
1A	1.15	9.2	3.34	147
1C	0.0117	NA	334	30
2A	1.13	9.0	3.33	204
2C	0.0112	NA	331	31
3A	1.11	8.9	3.35	177

The measured and calculated resonant frequency of the individual resonators is shown in Table 4.2. Resonant frequencies were measured using the impedance analyzer and calculated from component values using

$$f = \frac{\sqrt{\frac{1}{\mathcal{C}\mathcal{L}} - \left(\frac{\mathcal{R}}{\mathcal{L}}\right)^2}}{2\pi}. \tag{4.1}$$

The system was excited using a Agilent 33522A function generator with 50 Ω output impedance set to sine wave output. The function generator was connected to one turn through the first core. An inductor with inductance 1.21 mH and resistance 10.5 Ω was placed in series with the source to reduce the coupling to the resonant system so as to minimize interfere with its behaviour. The connection to the source and the series inductor

Table 4.2: Resonant frequency of each cell used to build five cell system

Cell	Measured Resonant Frequency [kHz]	Calculated Resonant Frequency [kHz]
1A	81.1	81.2
1C	80.8	80.7
2A	81.9	82.0
2C	82.7	80.2
3A	82.3	82.5

can be seen on the left side of Fig. 4.3. The frequency of the function generator was swept from 0 to 300 kHz and the transmission response was measured on a Tektronix DPO5054 oscilloscope coupled to one turn through the last core using a 10 MΩ impedance ×10 probe.

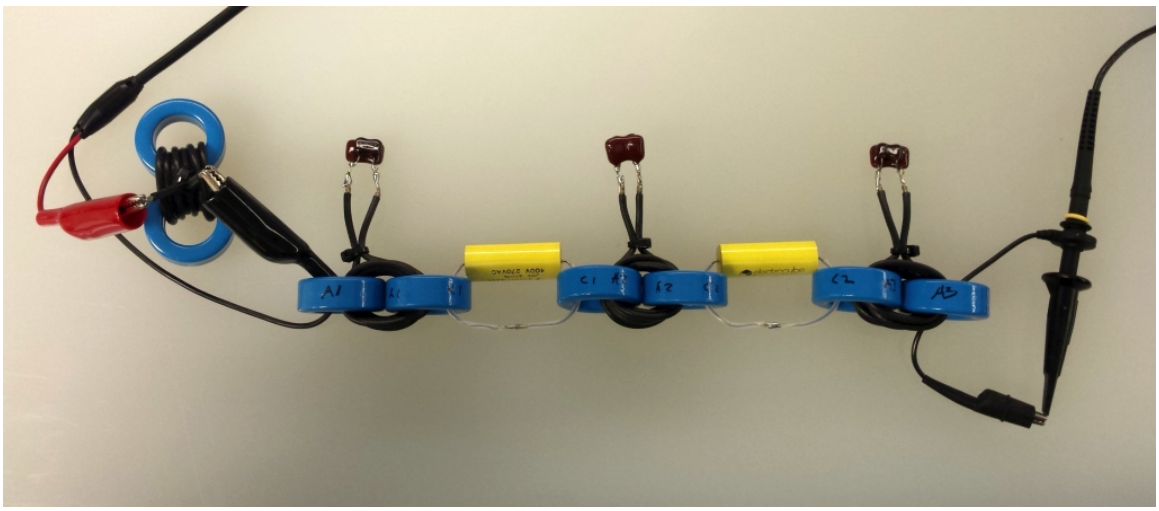

Figure 4.3: Transmission measurement setup of five cell system showing input from function generator on left and oscilloscope probe on right

Synchronizing the oscilloscope to the sweep trigger allowed the transmission spectrum to be observed as shown in Fig. 4.4.

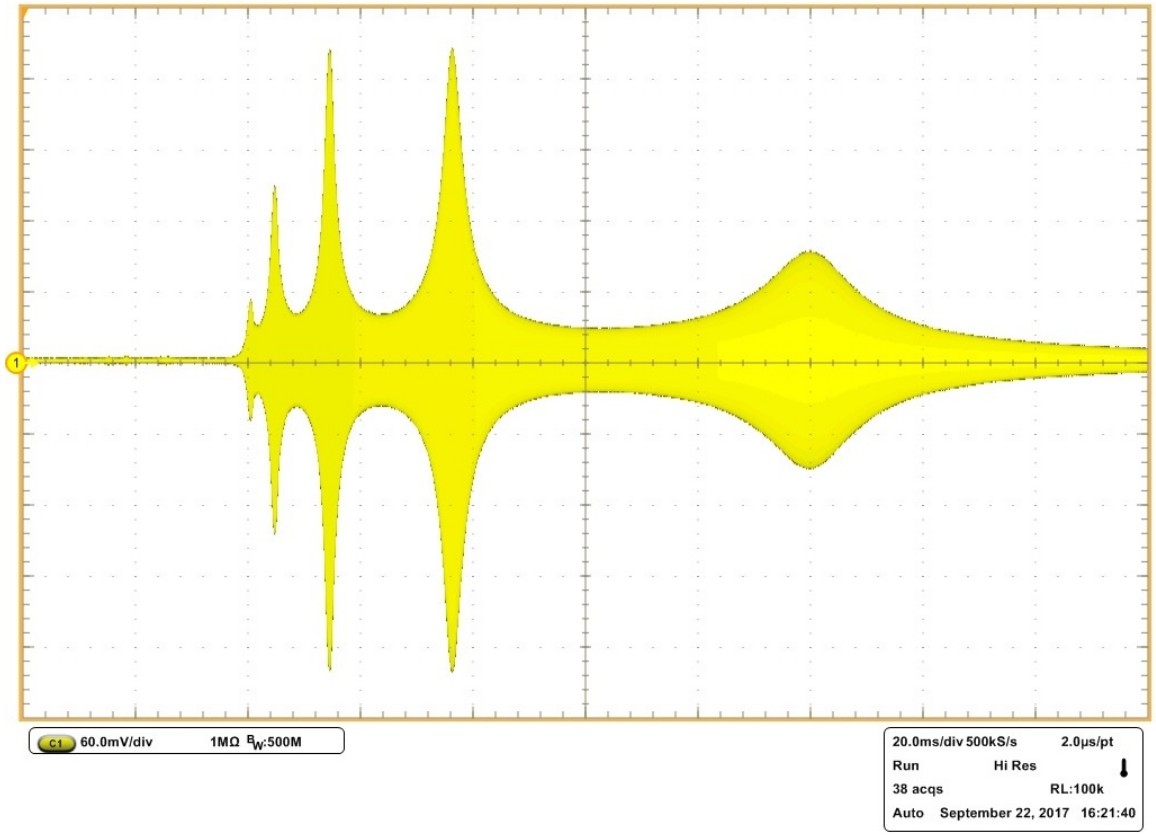

Figure 4.4: Oscilloscope screen capture of last cell voltage, in arbitrary units, vs. swept input frequency, with 30 kHz per major division, depicting transmission spectrum of five cell system

For better clarity, the oscilloscope was configured to display the Fourier spectrum of the signal as shown in Fig. 4.5

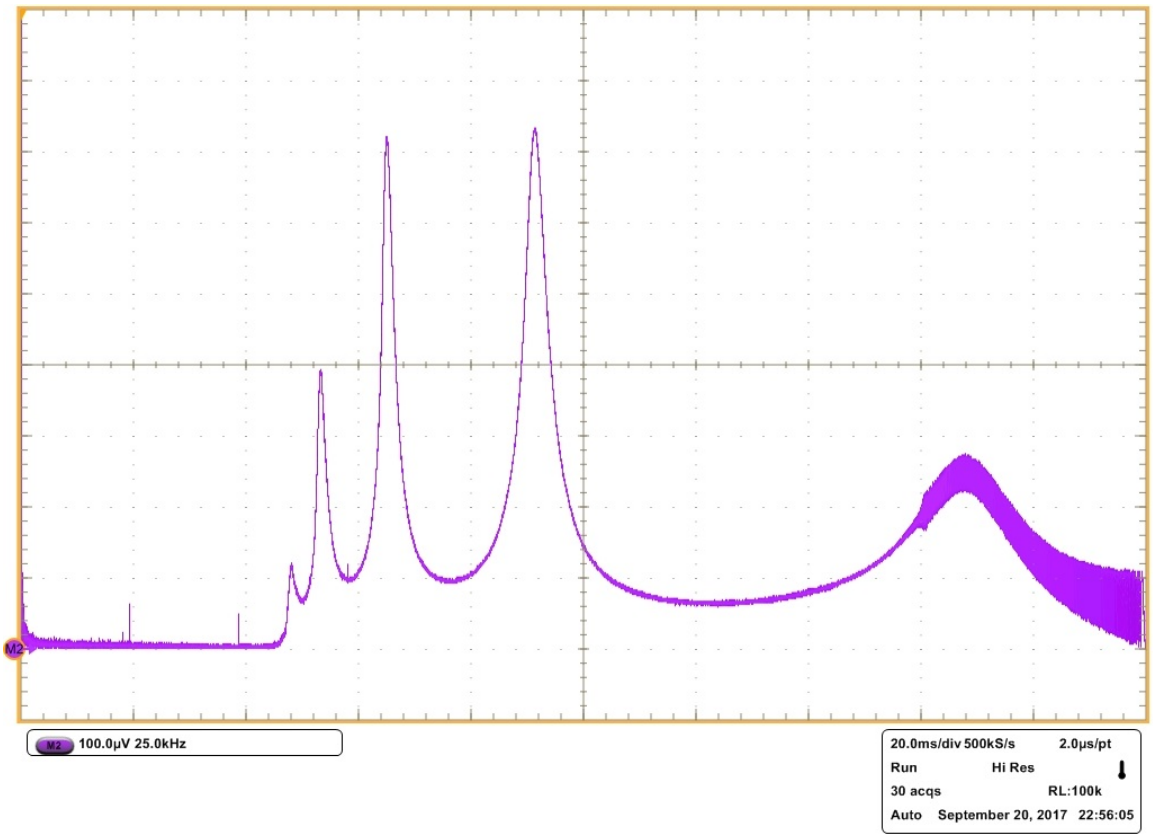

Figure 4.5: Oscilloscope screen capture of Fourier transform of last cell voltage, in arbitrary units, vs. frequency, with 25 kHz per major division, more clearly depicting transmission spectrum of five cell system

The the frequency of the peaks corresponding to each mode were measured and are shown in Table 4.3

Table 4.3: Measured mode frequencies

Mode	Frequency [kHz]
$\pi/6$	60.1
$\pi/3$	66.5
$\pi/2$	81.3
$2\pi/3$	114.2
$5\pi/6$	209

A plot of these data compared to the theoretical dispersion curve given by Eq 2.5 is

shown in Fig. 4.6. Good agreement was found between the measured and theoretical values with least squares fit parameters of $k = 0.979$, $f_1 = 81.7$ kHz, and $f_2 = 81.3$ kHz.

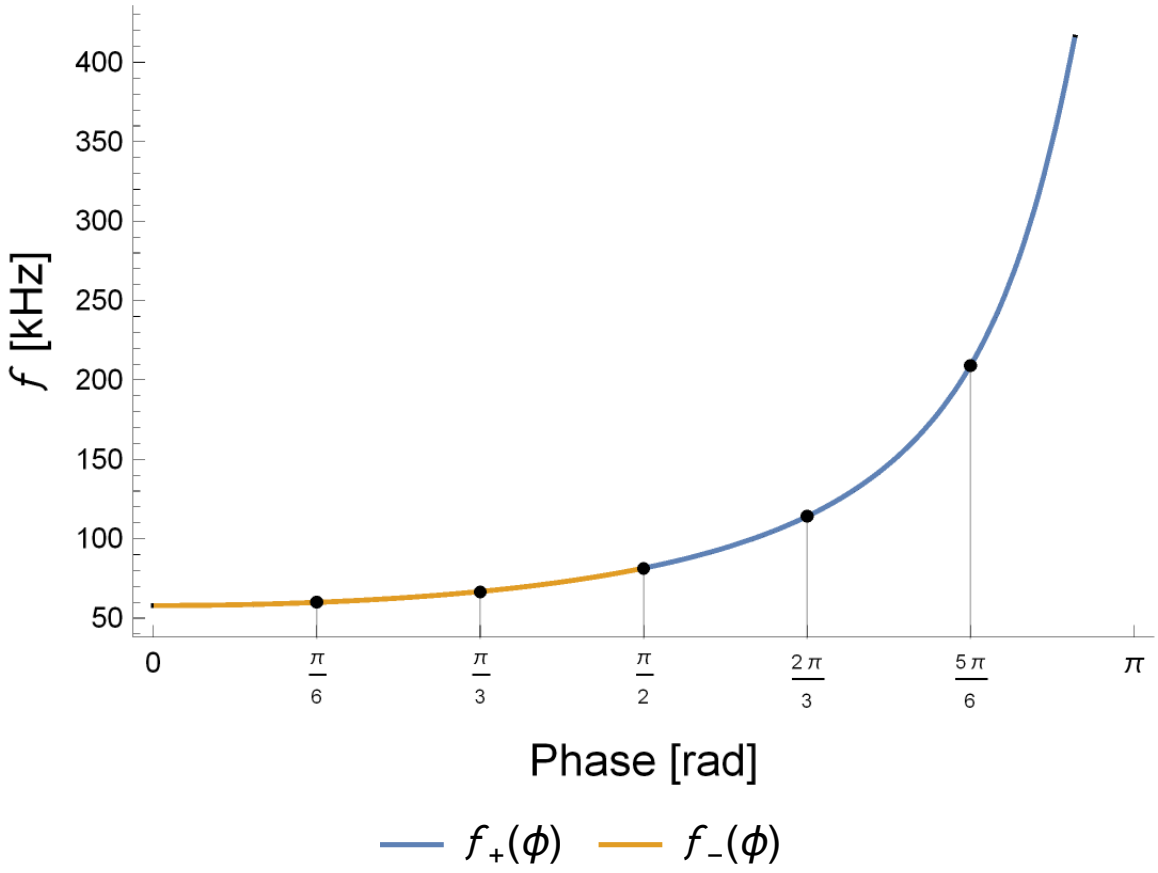

Figure 4.6: Mode frequencies measured on five cell system, shown as dots, plotted with theoretical dispersion curve shown as yellow and blue lines with least squares fit parameters of $k = 0.979$, $f_1 = 81.7$ kHz, and $f_2 = 81.3$ kHz

The ratios of the rms voltages of a single turn on each cell to the rms voltage of a single turn on the first cell were measured for each mode frequency; these are plotted in Fig. 4.7. Note the even distribution of the voltages on the odd numbered capacitors in the $\pi/2$ mode.

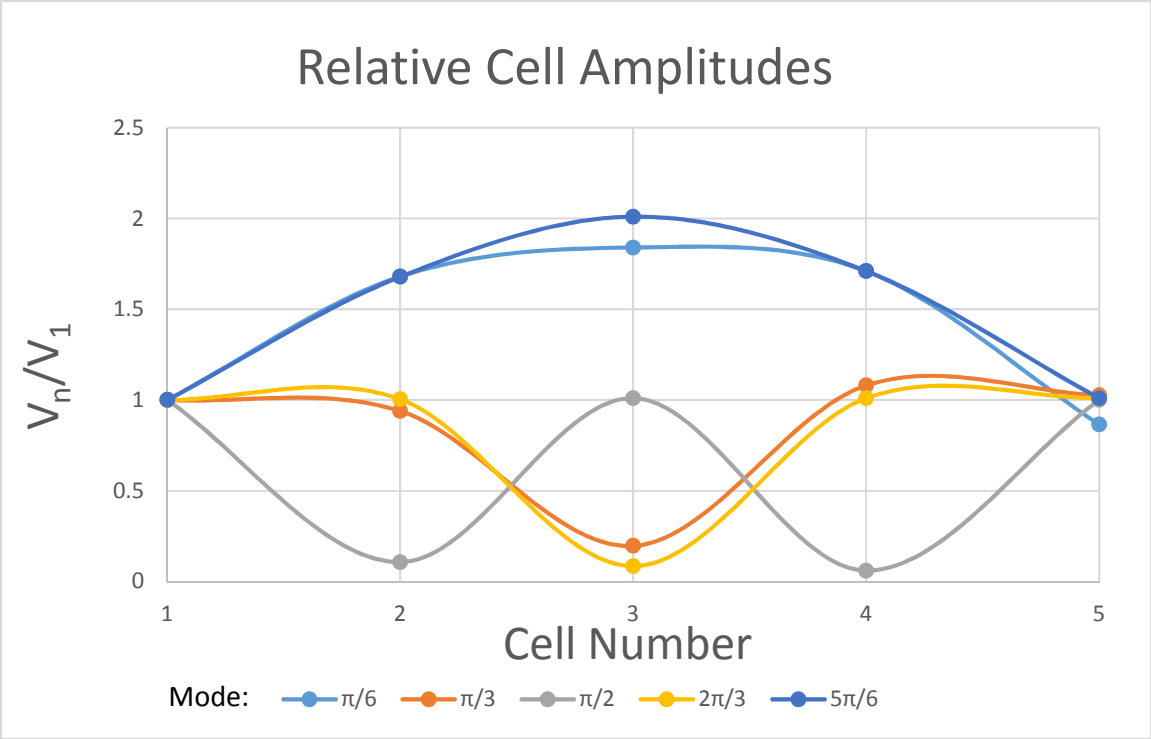

Figure 4.7: Measured spatial mode distribution of five cell benchtop model

To evaluate the transient response of the system in the $\pi/2$ mode the pulse generator frequency was set 81.3 kHz and "Burst Mode" was enabled. Bursts of 100 pulses were delivered to the system and the response was measured with a 10 MΩ impedance ×10 probe connected to one turn coupled to odd cell inductors. Figures 4.8, 4.9, and 4.10 show the system's transient response with 20 μs, 50 μs, 200 μs, per division respectively; in each figure the voltage on the first, third, and fifth capacitor can be observed increasing to their steady state values.

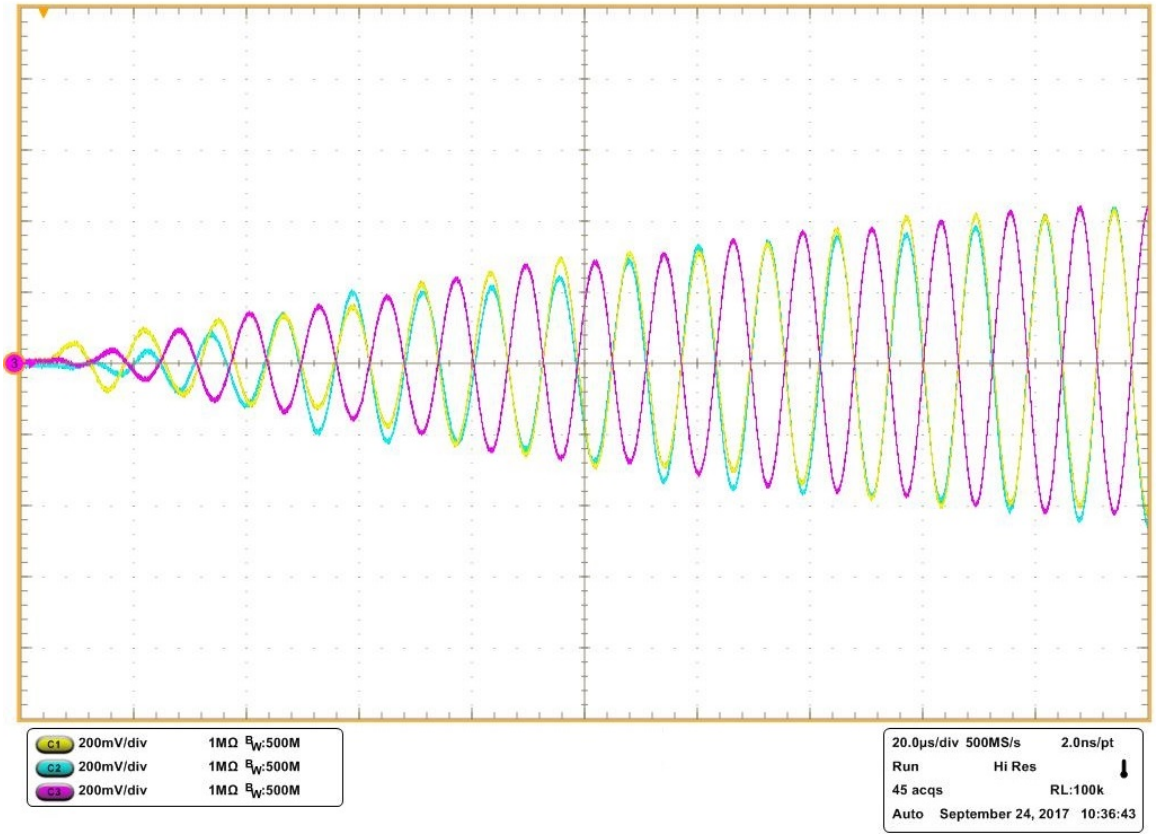

Figure 4.8: Oscilloscope screen capture of transient response of five cell system showing voltage across first capacitor (Yellow, 200 mV/div), third capacitor (Magenta, 200 mV/div), and fifth capacitor (Cyan, 200 mV/div) increasing with time (20 μs/div)

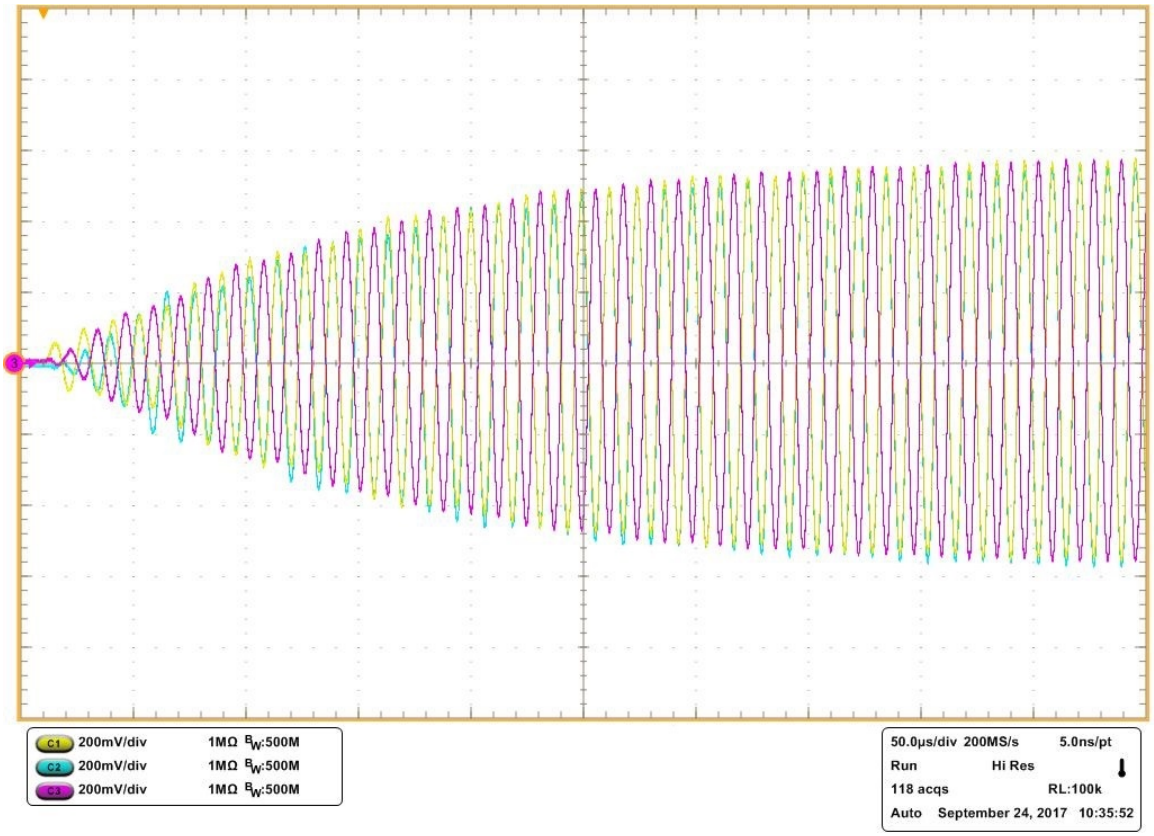

Figure 4.9: Oscilloscope screen capture of transient response of five cell system showing voltage across first capacitor (Yellow, 200 mV/div), third capacitor (Magenta, 200 mV/div), and fifth capacitor (Cyan, 200 mV/div) increasing with time (50 μs/div)

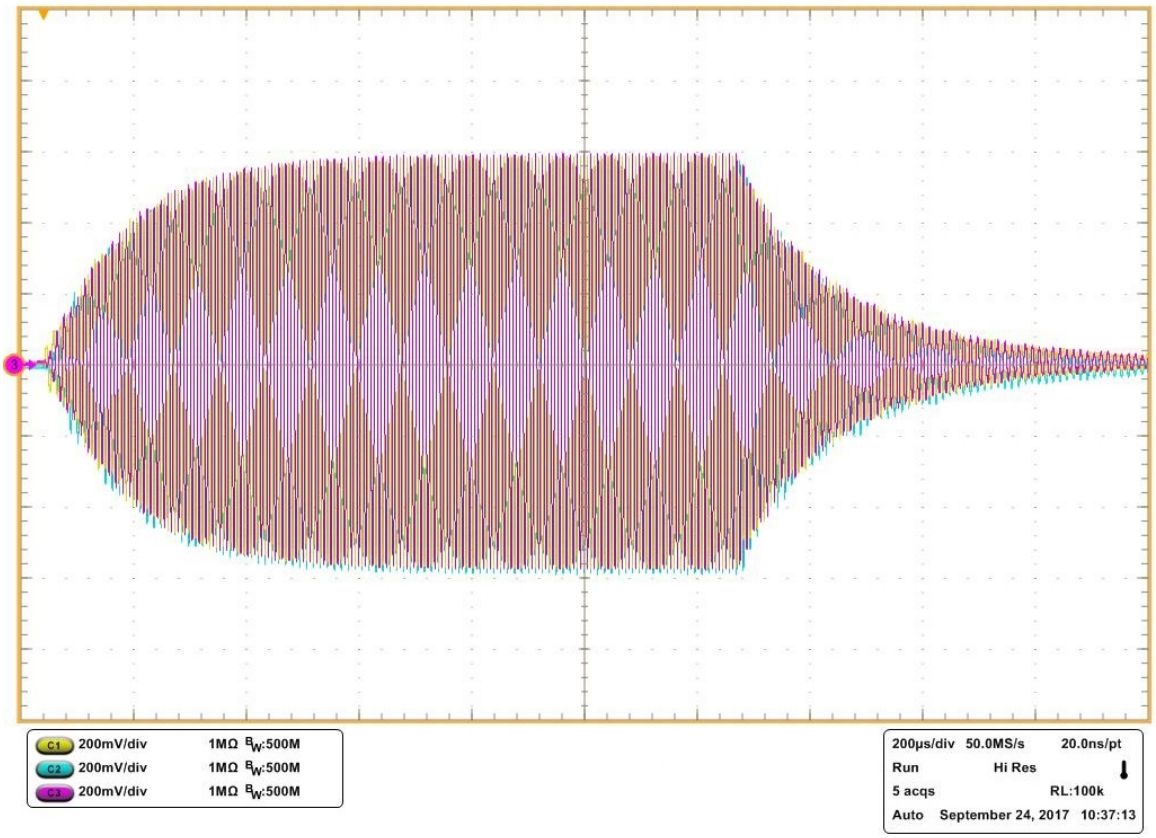

Figure 4.10: Oscilloscope screen capture of transient response of five cell system showing voltage across first capacitor (Yellow, 200 mV/div), third capacitor (Magenta, 200 mV/div), and fifth capacitor (Cyan, 200 mV/div) increasing with time (200 μs/div)

To increase the peak voltage on the active cell capacitors, an impedance matching transformer was added between the generator and the first core of the system to better match the 50 Ω output of the function generator to the input impedance of the system. This increased the rms voltage across the three active cell capacitors to 23 V, 24.5 V and 24.5 V respectively.

To demonstrate that interconnecting the active cells would not interfere with the performance of the resonant system, the three active cell capacitors were connected in series. The connections to the middle active cell were reversed so that all three signals would be in phase. This configuration is shown in Fig. 4.11. The red and black alligator clips on the left

provide input power from the function generator to the impedance matching transformer. The yellow ringed probe on the far left monitors the input voltage. The blue ringed probe on the right monitors the series output voltage. The blue wires provide the series connection. The green wire transfers power from the impedance matching transformer to the system.

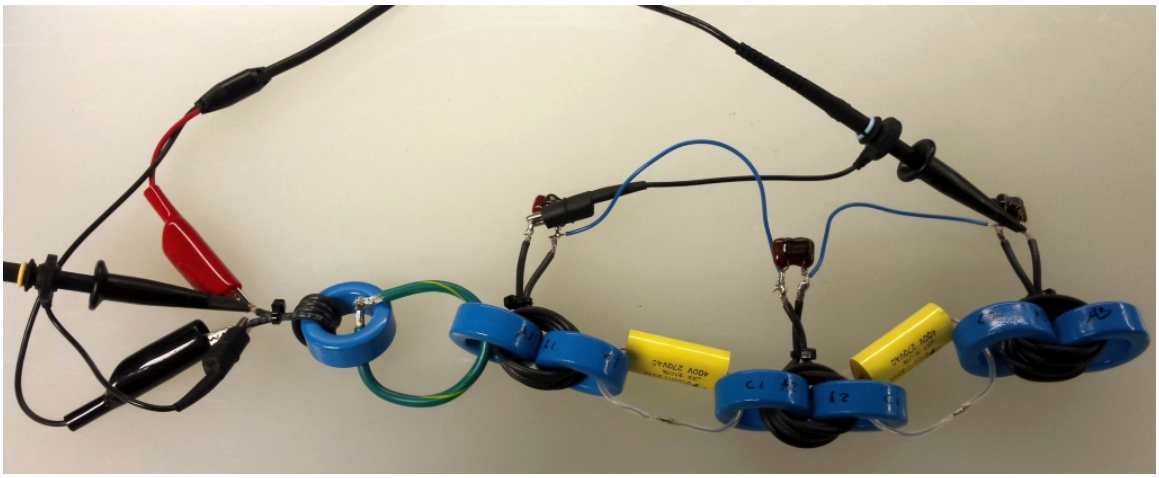

Figure 4.11: Five cell system configured for ac output

An equivalent schematic of this system is shown in Fig. 4.12

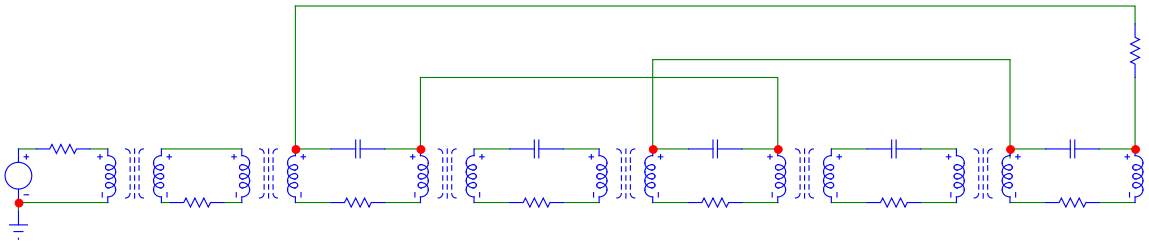

Figure 4.12: Five cell system configured for ac output

With the function generator programmed to 7 V_{rms}, 3.5 V_{rms} was measured on the input of the impedance matching transformer (with the remaining 3.5 V_{rms} being across the internal impedance of the function generator.) The series output voltage of the system was measured at 71.6 V_{rms} (101 V_{peak}) as shown in figure. 4.13.

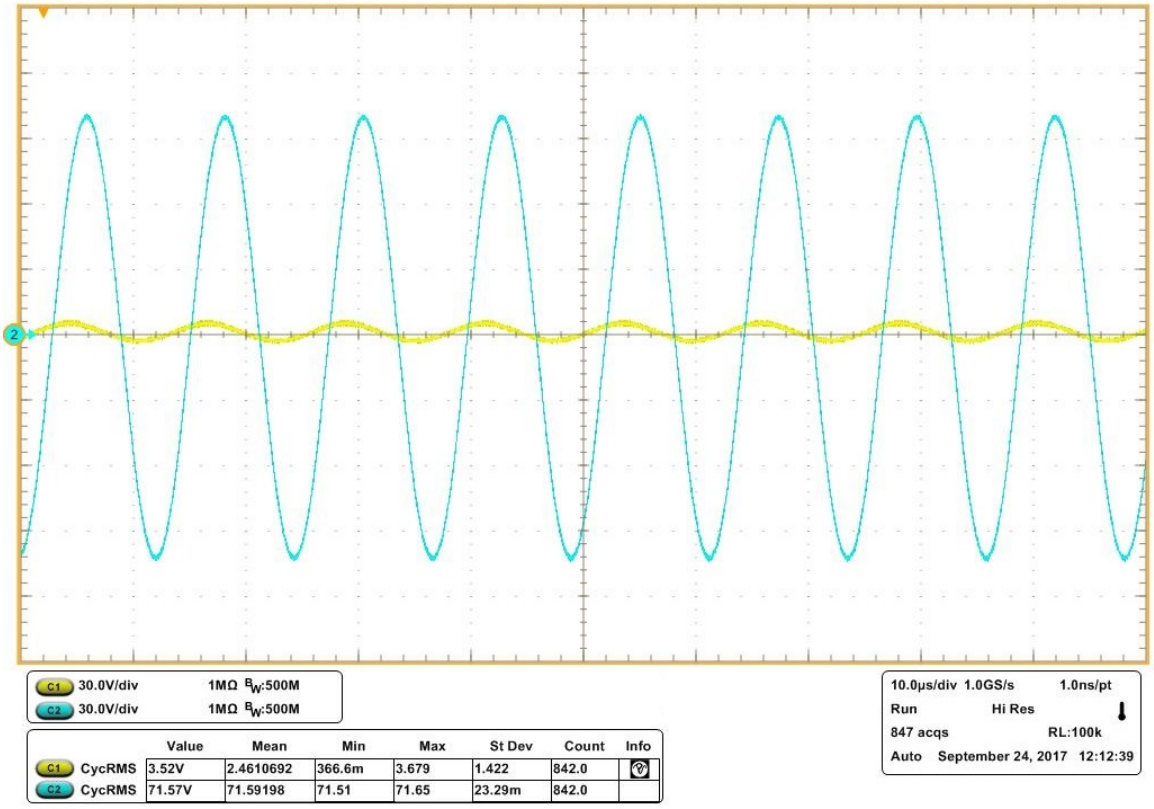

Figure 4.13: Oscilloscope screen capture of input voltage (Yellow, 30 V/div) and output voltage (Cyan, 30 V/div) of five cell system configured for ac output vs. time (10 μs/div)

To demonstrate that using the active cells to charge energy storage capacitors through rectifiers would not interfere with the performance of the resonant system, the series connections between cells were removed, and voltage doubler circuits were connected to each of the three active cell resonant capacitors. The voltage doublers were each made using two 1N4005 diodes and two 1 μF, 200V polypropylene capacitors. The 1N4005 diodes are less than ideal for this application due to their slow standard recovery time. The outputs of the voltage doubler circuits were then connected in series to generate high voltage. In a pulsed power modulator application the series connections between the voltage doublers would be made with semiconductor switches once the voltage doubler capacitors have been sufficiently charged. A single voltage doubler circuit connected to the first active cell resonant capacitor

is shown Fig. 4.14. The scope probe seen in the upper right of Fig. 4.14 is connected to the output terminals of the doubler circuit.

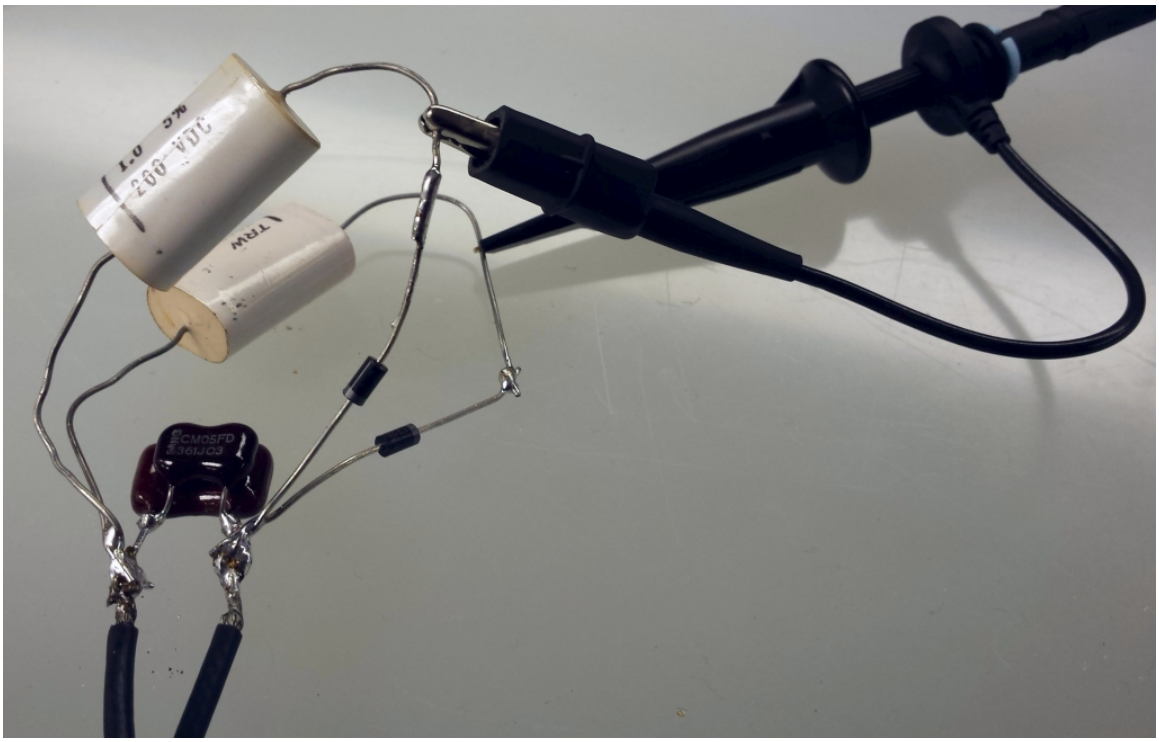

Figure 4.14: Voltage doubler circuit powered by first cell resonant capacitor

The completed circuit with all three voltage doublers is shown in Fig. 4.15. Schematic of this circuit is shown in Fig. 4.16.

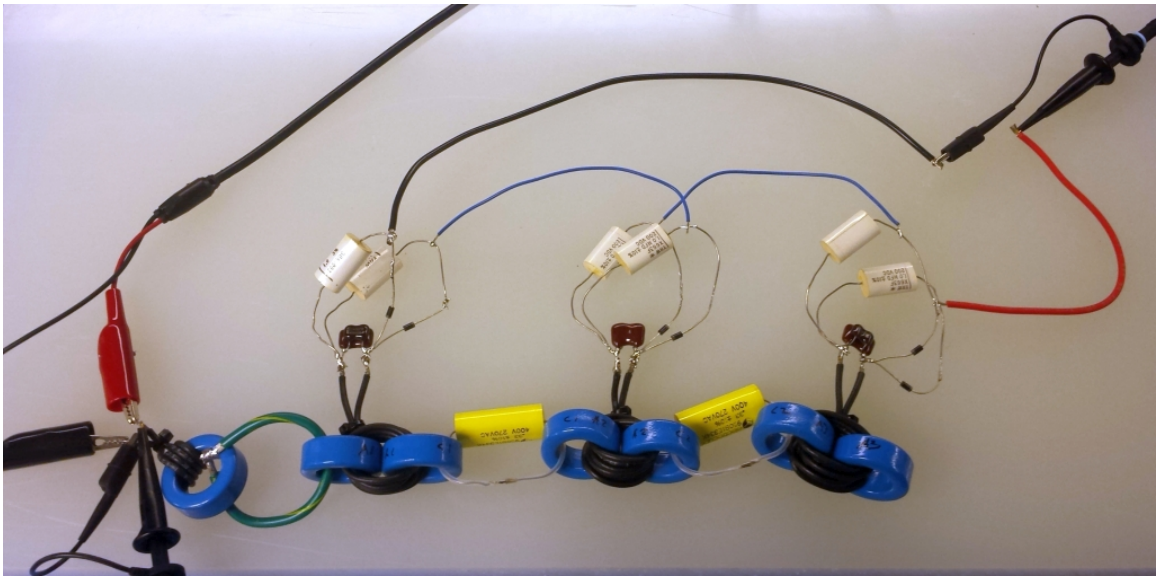

Figure 4.15: Five cell biperiodic resonant system powering three voltage doublers.

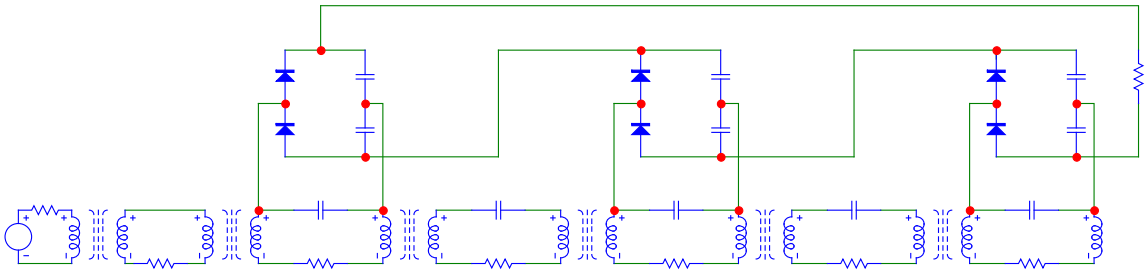

Figure 4.16: Schematic of five cell biperiodic resonant system with voltage doublers

With the three voltage doublers connected, the input voltage drooped from 3.52 V_{rms} down to 3.46 V_{rms}, possibly from the losses in the 1N4005 diodes. The leakage current of the diodes, though only about 5 μA, creates a significant drain on the 1 μF capacitors. Despite this, the output voltage from the three voltage doublers in series reached 194 V_{dc} in the steady state condition as shown in Fig. 4.17.

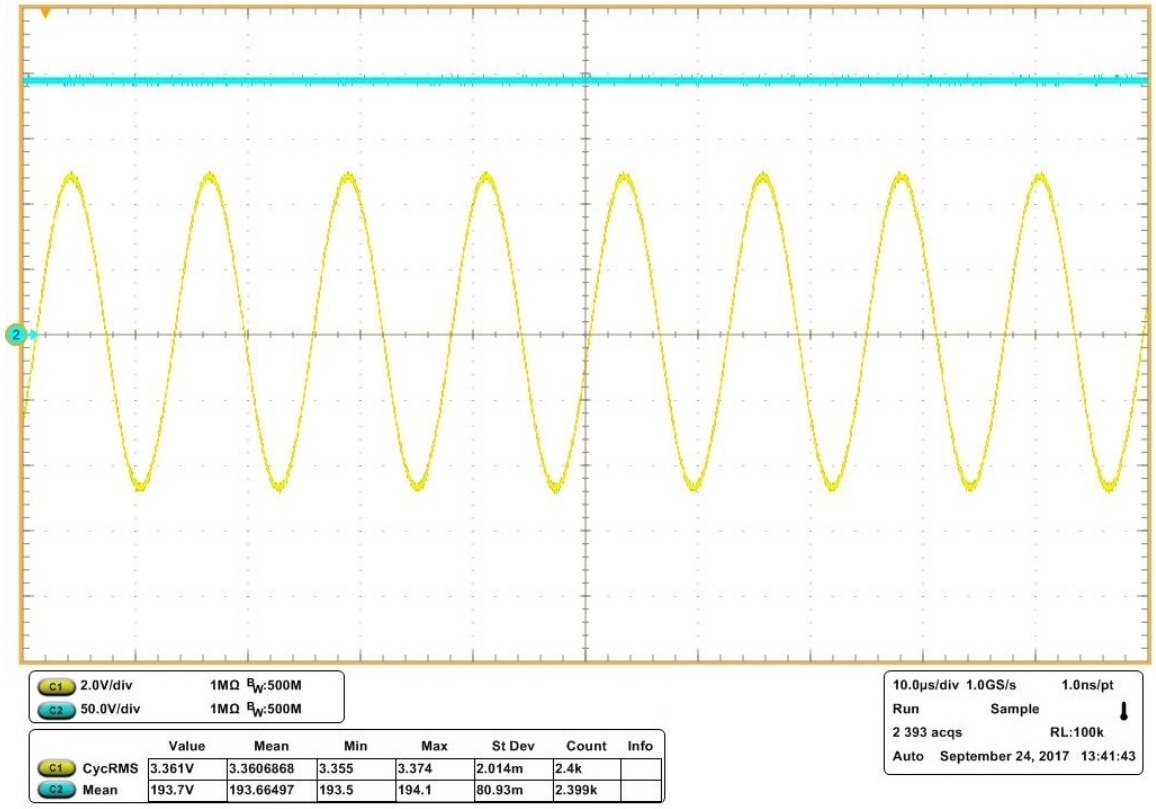

Figure 4.17: Input voltage (Yellow, 2 V/div) and high voltage dc output (Cyan, 50 V/div) vs. time (10 μs/div) of five cell biperiodic resonant system powering three voltage doublers.

The impulse response of the system can be seen in Fig. 4.18 and Fig. 4.18. Note the voltage decreasing between pulses due to discharge of the capacitors from diode leakage current.

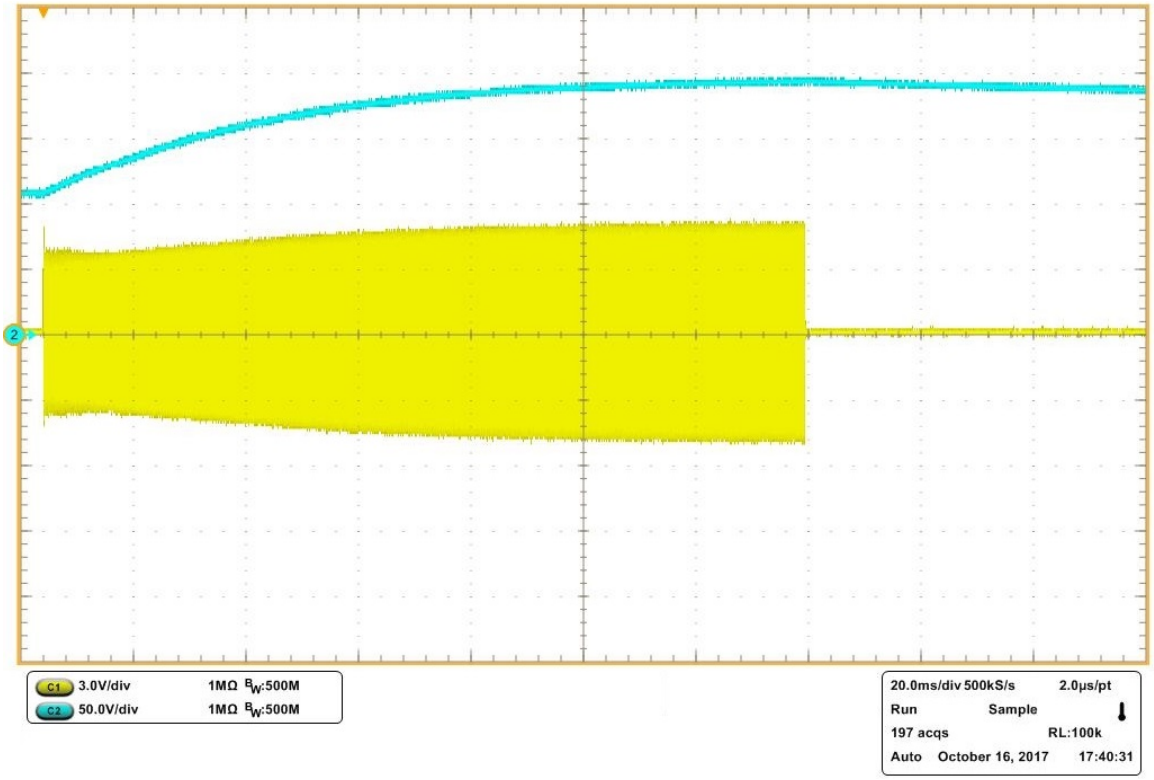

Figure 4.18: Response of dc voltage (Cyan, 50 V/div) to input transient (Yellow, 3 V/div) vs. time (20 ms/div)

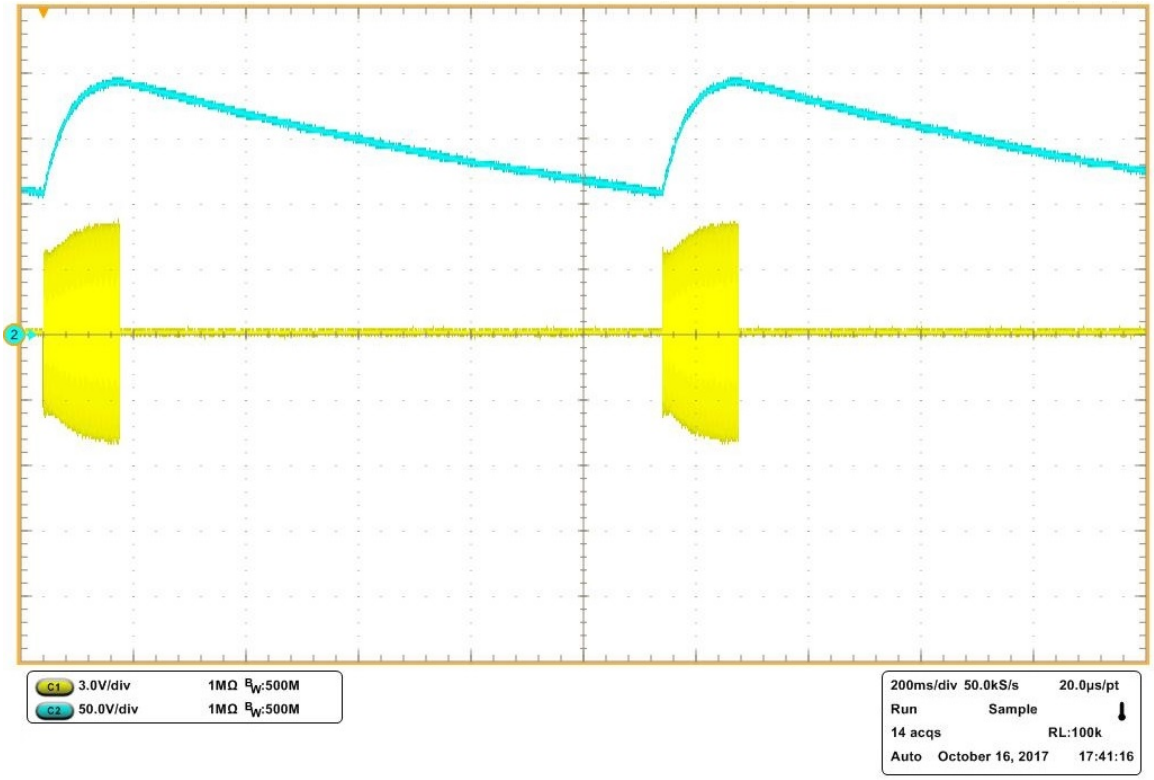

Figure 4.19: Response of dc voltage (Cyan, 50 V/div) to input transient (Yellow, 3 V/div) vs. time (200 ms/div)

To turn this system of coupled oscillators into a Marx generator, three International Rectifier IRF840 MOSFETs were added, one to each of the voltage doublers as shown in the schematic in Fig. 4.21 and the photo in Fig. 4.20.

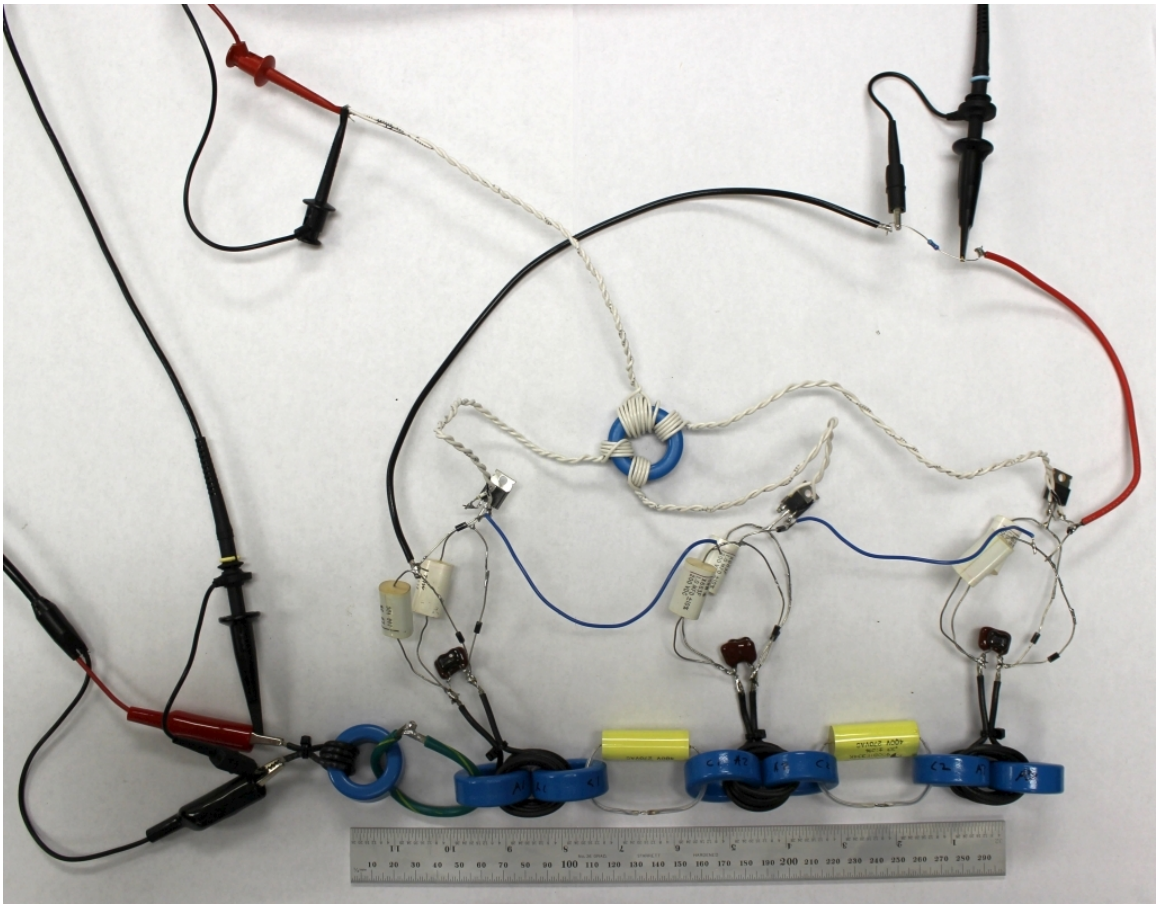

Figure 4.20: Five cell biperiodic cascaded transformer charging a three stage solid state Marx generator. Input power from function generator and input voltage measurement probe shown in left side of image. Gate drive input shown in upper left in image. Load resistor and output voltage measurement probe shown in upper right in image.

To simplify the build of the model, a hand wound transformer was used to transfer the gate drive signals to the MOSFETs while providing isolation between the separate MOSFETs and ground. The gate drive transformer is shown in the center of Fig.4.20. The input to the gate drive transformer was provided by a Berkeley Nucleonics Corp BNC 575-4C. In a practical design with much higher voltage output requiring more gate drive isolation, the gate drives could be powered off the coupled resonators and triggered via fiber optic cable as with Adler's design [8].

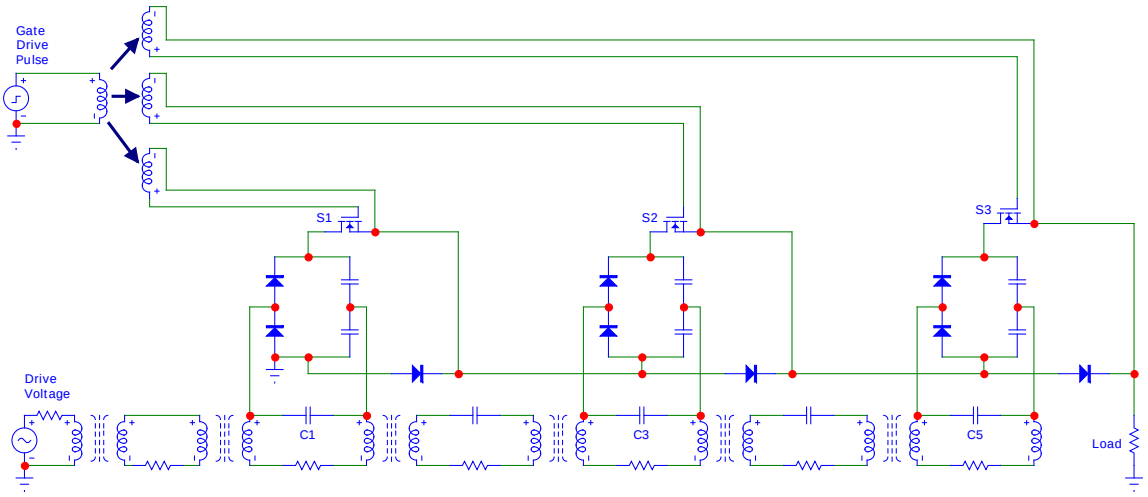

Figure 4.21: Schematic of five cell biperiodic cascaded transformers charging a three stage solid state Marx generator

Pulsed output voltage into a 4.7 kΩ resistive load is shown in Fig. 4.22.

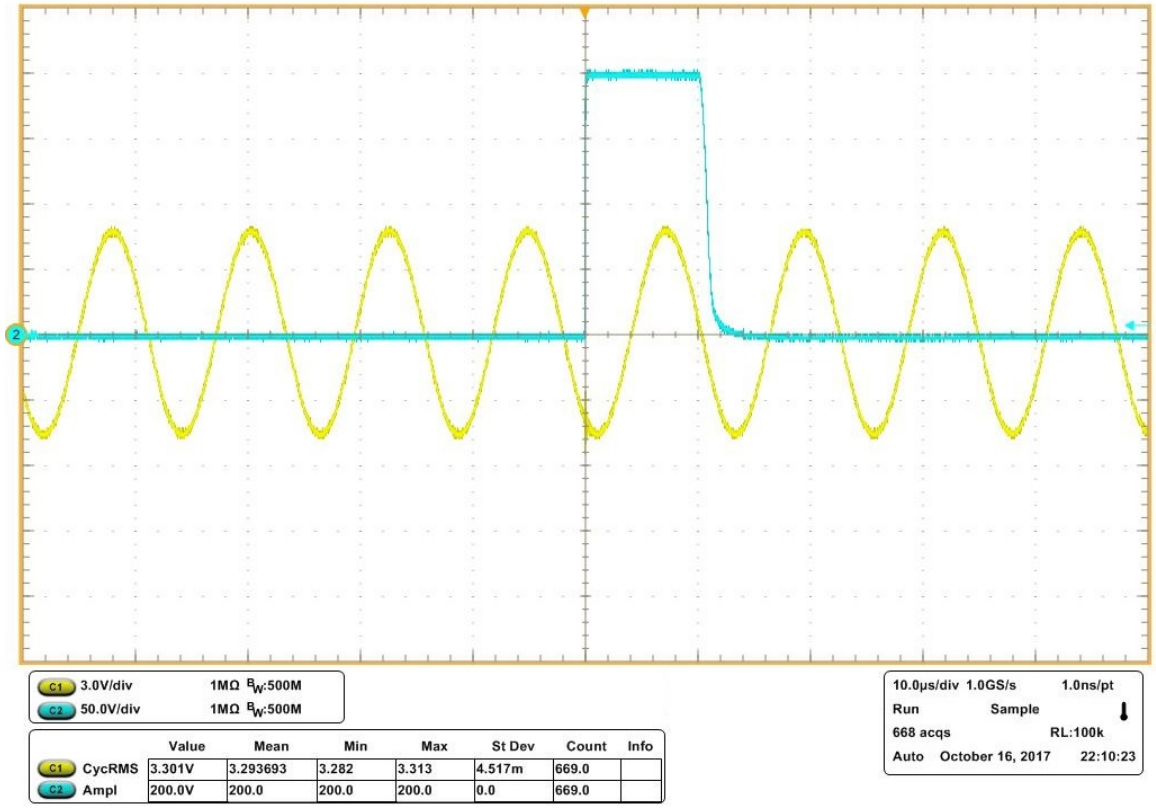

Figure 4.22: Marx Generator output (Cyan, 50 V/div) and input drive voltage (Yellow, 3 V/div) vs. time (10 μs/div)

Leading edge rise time is less than 100 ns as shown in Fig. 4.23.

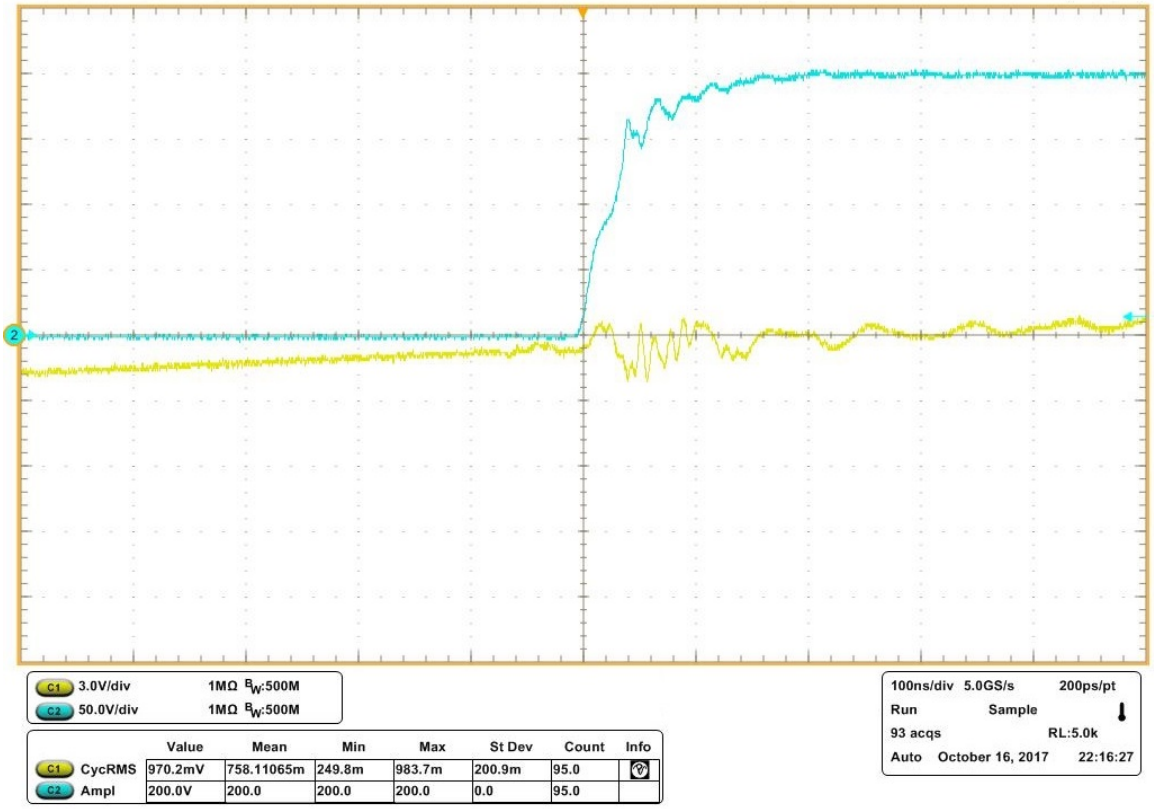

Figure 4.23: Expanded view of Marx generator output leading edge (Cyan, 50 V/div) and input drive voltage (Yellow, 3 V/div) vs. time (100 ns/div)

This simple model circuit has demonstrated that a system of coupled oscillators operating in the $\pi/2$ mode can be connected in series for high voltage ac, used to power rectifier circuits to charge capacitors for high voltage dc, or, with the addition of a switch in each active cell, charge a Marx generator. In each case the system is powered from one end by a power source that sits safely at ground potential.

4.2 SPICE SIMULATION OF MODEL

A SPICE model of this five cell resonator was constructed in Micro-Cap 11 using the previously measured component values in Table 4.1 [25]. The schematic of the simulation is shown in Fig. 4.24.

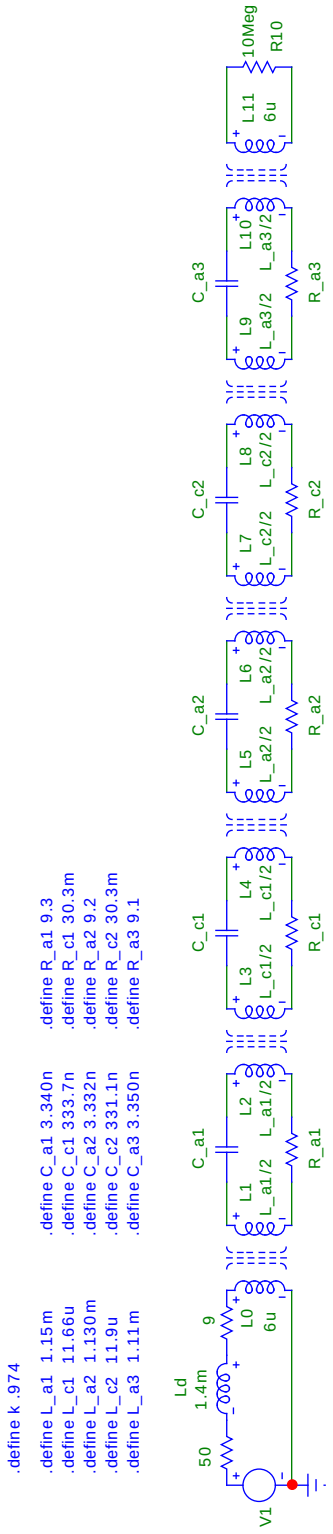

Figure 4.24: Schematic of five cell system used for SPICE simulation

The coupling constants, k, for all transformers were set equal and were adjusted so that the mode frequency spacings matched those measured on the physical system. A coupling constant around 0.97 was found to give a close match to the mode frequencies measure on the physical system. This is close to the value of 0.98 measured previously. The mode frequencies of the physical system and the SPICE simulated system with this coupling are listed in Table 4.4.

Table 4.4: Comparison of measured and simulated mode frequencies

Mode	Measured Frequency [kHz]	Simulated Frequency[kHz]
$\pi/6$	60.1	59.9
$\pi/3$	66.5	66.6
$\pi/2$	81.3	82.0
$2\pi/3$	114.2	113.2
$5\pi/6$	209	203

The transmission spectrum of the SPICE simulated system is shown in Fig. 4.25 and gives good agreement to the spectrum of the physical system shown earlier in 4.5.

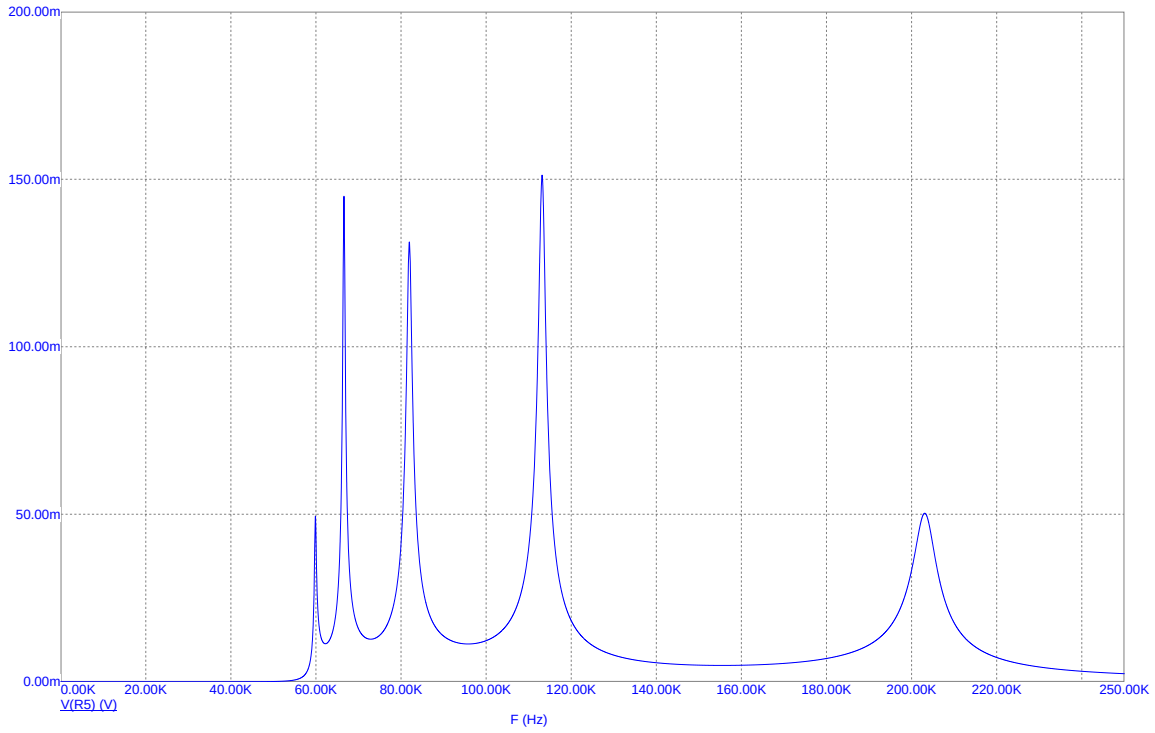

Figure 4.25: SPICE simulated mode spectrum of five cell system

The transient response of the SPICE simulated system is shown in Fig. 4.26 and is comparable to the transient response of the physical system shown earlier in 4.9.

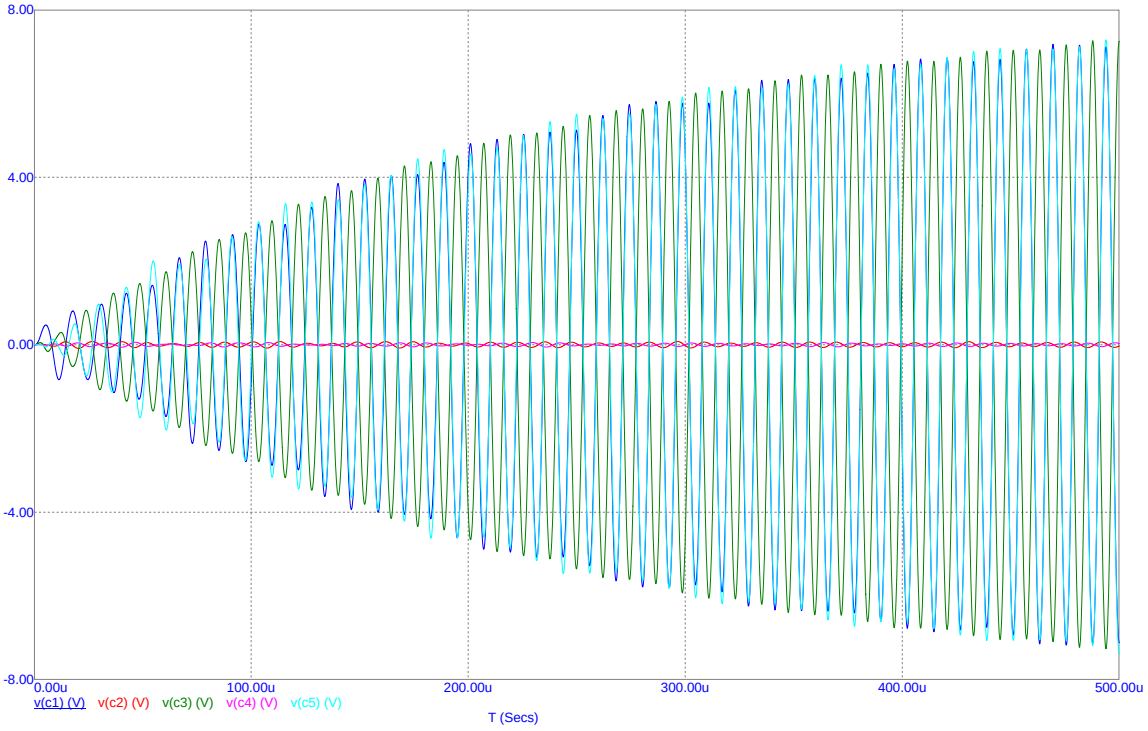

Figure 4.26: SPICE simulated transient response

To simulate a full Max circuit, MOSFET switches and simplified gate drive circuitry were added to the SPICE model as shown in Fig. 4.27.

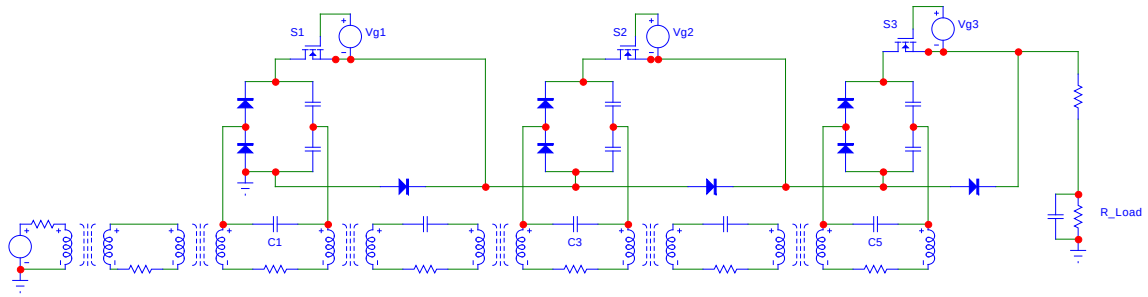

Figure 4.27: SPICE model with MOSFET switches for pulse simulation.

The active cell capacitor voltage envelopes and the pulse voltage applied to the load is shown in Fig. 4.28.

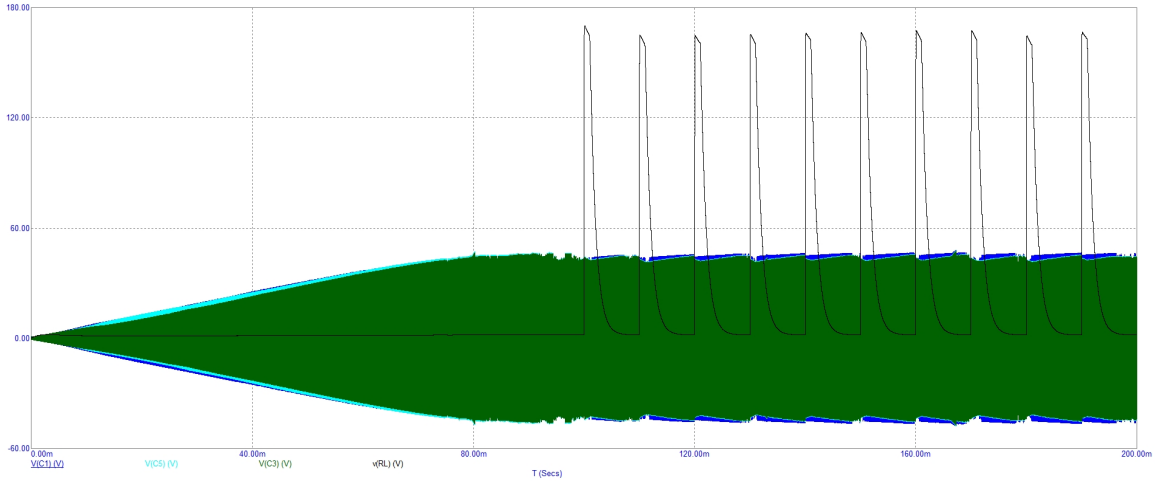

Figure 4.28: SPICE simulated pulse output voltage shown in black with active cell capacitor voltage envelopes shown in blue, cyan, and green.

The active cell resonant capacitors (C1, C3, C5) can be seen charging up for the first 80 mS. At 100 mS the MOSFETs turn on and deliver pulses to the load. After each pulse the energy in the resonant capacitors builds back up before the next pulse.

4.3 MATRIX ANALYSIS OF MODEL

From a design perspective, it is important to understand the properties of a resonant system before building it or even before creating a SPICE simulation. The analytical tools developed in Chapter 3 can be used to quickly calculate the modes for a finite resonant system for which we know the component values. Starting with the eigenvalue equation Eq. 3.11 and using the individual inductor and capacitor values in Table 4.1 we can solve the eigenvalue equation to calculate the mode frequencies. Recalling Fig. 3.1 we can see that $\mathcal{L}_n$ is the total inductance of cell n and the coupling $\mathcal{K}_{mn}$ is the coupling between the total inductance of cells n and m. Due to the way the inductors were wired and measured, the inductance recorded in Table 4.1 is already the total inductance for the cell. However in our circuit topology, the

transformer coupling is only to half of the total cell inductance of each cell. Therefore the coupling to the total inductance is half of the coupling to the transformer inductance used in the SPICE simulation. With this in mind, the values of $\mathcal{L}$, $\mathcal{C}$, and $\mathcal{K}$ can be determined.

$$\mathcal{L} = \begin{pmatrix} 1.15 \text{ mF} \\ 11.66\ \mu\text{F} \\ 1.13 \text{ mF} \\ 11.19\ \mu\text{F} \\ 1.11 \text{ mF} \end{pmatrix} \tag{4.2}$$

$$\mathcal{C} = \begin{pmatrix} 3.34 \text{ nC} & 0 & 0 & 0 & 0 \\ 0 & 334 \text{ nC} & 0 & 0 & 0 \\ 0 & 0 & 3.33 \text{ nC} & 0 & 0 \\ 0 & 0 & 0 & 33.1 \text{ nC} & 0 \\ 0 & 0 & 0 & 0 & 3.35 \text{ nC} \end{pmatrix} \tag{4.3}$$

$$\mathcal{K} = \begin{pmatrix} 1 & \frac{0.97}{2} & 0 & 0 & 0 \\ \frac{0.97}{2} & 1 & \frac{0.97}{2} & 0 & 0 \\ 0 & \frac{0.97}{2} & 1 & \frac{0.97}{2} & 0 \\ 0 & 0 & \frac{0.97}{2} & 1 & \frac{0.97}{2} \\ 0 & 0 & 0 & \frac{0.97}{2} & 1 \end{pmatrix} \tag{4.4}$$

Substituting the values in Eqs. 4.2, 4.3, 4.4 into Eq. 3.11, solving for the eigenvalues, and taking the square root of the reciprocal of the eigenvalues gives the angular frequency, ω, of each mode. Finally, dividing the angular frequencies by 2π gives the cycle frequencies for each mode. The values calculated by this method are shown in Table 4.5 along with the values measured on the model and the values found with the spice simulation. The good agreement between these three data sets show that one can efficiently and accurately predict

system performance using matrix formulation and SPICE analysis.

Table 4.5: Comparison of Mode Frequencies [kHz]

Mode	Measured [kHz]	Simulated [kHz]	Calculated [kHz]
$\pi/6$	60.1	59.9	60.3
$\pi/3$	66.5	66.6	67.1
$\pi/2$	81.3	82.0	81.9
$2\pi/3$	114.2	113.2	113.9
$5\pi/6$	209	203	204.6

We have shown that a simple resonant cascaded transformer can be made from common components and used to charge a small Marx generator. Its performance matches that shown by both matrix analysis and SPICE simulation validating these design tools. We will uses these tools in Chapter 5 to design a larger system with a more practical application.

CHAPTER 5

PRACTICAL DESIGN EXAMPLE

Now that we have developed and validated tools for studying the topology in Fig. 1.15 let us consider a practical application. Electron tube manufacturer e2V, now part of Teledyne, recently released their MG7095 S-band magnetron with specifications per Table 5.1 [26].

Table 5.1: Selected properties of Teledyne e2V MG7095 magnetron

Frequency Range	2993 to 3002 MHz
Maximum Peak Output Power	3.1 MW
Maximum Average Input Power	8.0 kW
Maximum Pulse Width	5.0 μs
Peak Anode Voltage	52 kV
Peak Anode Current	120 A
Maximum Heater Power	180 W

Suppose we want to operate this magnetron at a conservative 2.5 MW pulse power output running at 45 kV pulse voltage and 110 Amp pulse current with an average output power of 5 kW with a pulse width of 4 μS. Knowing the total output voltage, 45 kV, we can choose voltage per stage to get the corresponding number of stages. First we should decide whether MOSFETs or IGBTs are more appropriate. MOSFETs tend to have faster switching times but IGBTs tend to have higher voltage ratings. With our low rep rate of 500 Hz and reasonable rise time requirement, IGBTs should have sufficient performance while keeping the number of stages low. Currently 6 kV IGBT devices are available but 4 kV and

4.5 kV are a little more common. Using a 4 kV rated device such as IXYS part IXEL40N400 derated to 2 kV would require 23 Marx stages driven by 23 active resonant cells. Using the PI/2 mode where every other cell is empty means there would be a total of 45 cells in the resonant system and the system would have 45 distinct modes.

Next we pick the peak resonant voltage of our active cells. In principle the designer does not have to make the peak voltage of the resonant capacitor in the active cells equal to the Marx stage voltage. A transformer, voltage divider, or voltage multiplier could be used increase or decrease the voltage to the appropriate voltage for charging the Marx energy storage capacitors. Making the peak voltage of the active cell resonators half of the Marx stage voltage allows for voltage doubler circuit to be used to achieve full wave rectification using only two diodes. As discussed earlier, we want to charge our Marx pulse capacitors to 2 kV so we would want the peak voltage on our resonant capacitors to be 1 kV.

We must now decide how much energy we wish to store in the active resonant cells. When discussing stored energy and losses in resonators it is useful to discuss the *quality factor* or Q of the system. The Q of a resonant system is defined as 2 π times the energy stored in the system divided by the energy dissipated per cycle. In terms of frequency and average power lost this becomes

$$Q \equiv \frac{2\pi f E_{\text{stored}}}{P_{\text{lost}}} \tag{5.1}$$

The efficiency, η, of a resonant system can be expressed in terms of Q_{load} where all losses are due to the load and Q_{res} where all the losses are from the resonator components.

$$\eta = \frac{1}{\frac{Q_{\text{load}}}{Q_{\text{res}}} + 1} \tag{5.2}$$

Alternately in terms of Q_{tot}, which is the Q including all losses, and Q_{res} the efficiency can

be expressed as

$$\eta = 1 - \frac{Q_{\text{tot}}}{Q_{\text{res}}} \tag{5.3}$$

From Eq. 5.2 we can see that it is desirable, for good efficiency, that Q_{res} be large compared to Q_{load}. So we should not pick a Q_{load} that is so large we are unable to economically build the circuit with an even larger Q_{res}. On the other hand if Q_{load} is too small energy will not propagate properly down the structure properly and we will have an uneven voltage distribution on the Marx stages. Let us proceed to investigate a Q_{tot} equal to 30.

Our next step is to determine the capacitor and inductor values of the active cells using the peak resonator voltage and the total Q we just determined. We know the stored energy in each of our active cells is

$$E_{\text{stor}} = \frac{1}{2} C_a V^2 \tag{5.4}$$

where V is the peak voltage on our active cell capacitors. Combining Eqs. 5.1 and 5.4 and solving for the capacitance gives

$$C_a = \frac{Q P_{\text{lost}}}{\pi f V^2} \tag{5.5}$$

with corresponding cell inductance of

$$L_a = \frac{V^2}{4\pi f Q P_{\text{lost}}} \tag{5.6}$$

and cell characteristic impedance of

$$Z \equiv \frac{V}{I} = \sqrt{\frac{L}{C}} = \frac{V^2}{2(P_{\text{lost}}\, Q)} \tag{5.7}$$

which we can use to get the peak active cell resonator current

$$I = \frac{2 P_{\text{lost}}\, Q}{V} \tag{5.8}$$

Inductor and capacitor component values for the system design can be calculated using Eqs. 5.5 and 5.6. We start by determining the power lost, P_{lost}, from each active cell resonator to the magnetron and to parasitic component losses. As mentioned above, we wish to deliver 5 kW of average power to the magnetron. We add to this the 180 W of filament power to get 5180 W of power lost from active cell resonators to the load. Adding ten percent for budgeted component parasitic losses brings us to 5698 W of total power lost. To get the power lost per active cell, we divide by the number of active cells, 23, to get 248 W lost per active cell. Using this power lost per active cell along with the previously chosen peak resonant voltage of 1 kV, $\pi/2$ frequency of 30 kHz, and loaded Q_a of 30, we can use equations Eqs. 5.5 and 5.6 to calculate the active cell capacitance and inductance to be 79 nF and 0.35 mH respectively. Using Eq. 5.7 the cell impendence will 67 Ω and the peak active cell resonator current will be about 15 A. Coupling cell inductance and capacitance values can be any convenient values the give the coupling cells the same resonant frequency as the active cells per Eq. 2.4 and satisfy other design requirements such as cost and minimum parasitic losses.

A system of 45 resonators with these parameters was simulated in SPICE. The loaded Q of the active cells, Q_a, was set to 30 as discussed above and the unloaded Q of the coupling cells ,Q_c, was set to 300. Coupling cell impedance was set equal to active cell impedance so that their voltages, and thereby stored energy, could be more easily compared. As discussed previously, the coupling cell impedance could be set independently of the active cell impedance to minimize losses in the coupling cells. Capacitor voltage amplitude for all 45 cells, with active cell loaded Qs equal to 30, are plotted in Fig. 5.1.

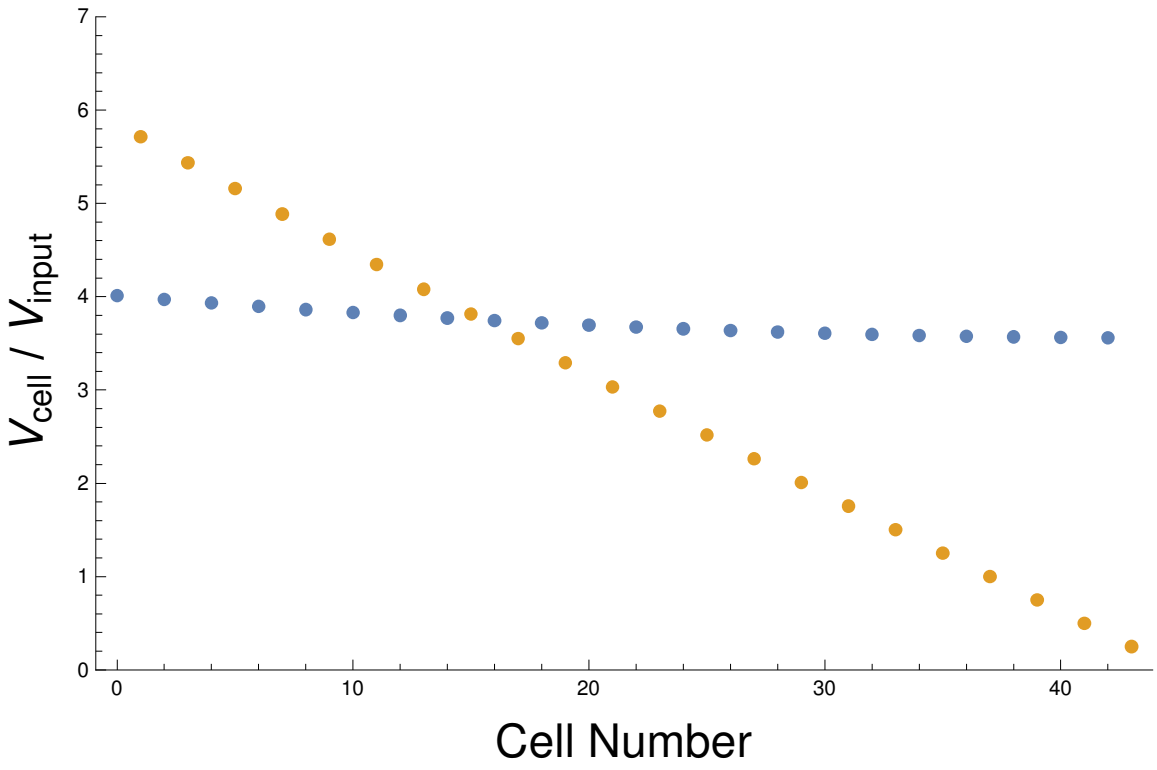

Figure 5.1: Spatial distribution of capacitor voltages for 45 cell resonant system operating in $\pi/2$ mode. Active cell voltages are shown in blue and coupling cell voltages are shown in yellow. Stored energy in active cells was adjusted so that the Q of each active cell equals 30 with design load applied. Coupling cell series resistance was adjusted to set the Q of each coupling cell to 300 to simulate small parasitic losses in coupling cell components.

Notice the mostly flat distribution with about 12% droop for the active (blue colored) cells and the very sloped distribution for the coupling (yellow colored) cells. The large voltage in the coupling cells is due to the phase shift in the active cells due to the high power flow from their relatively low loaded Q. The downward slope of the coupling cell distribution is due to each coupling cell transferring less power than the one before it. For much higher values of active cell loaded Q the voltage and stored energy in the coupling cells are near zero.

Increasing the loaded Q of the active cells to 60 decreases the voltage droop in the active

cells to 6% and reduces the voltage in the coupling cells by half as shown in Fig. 5.2.

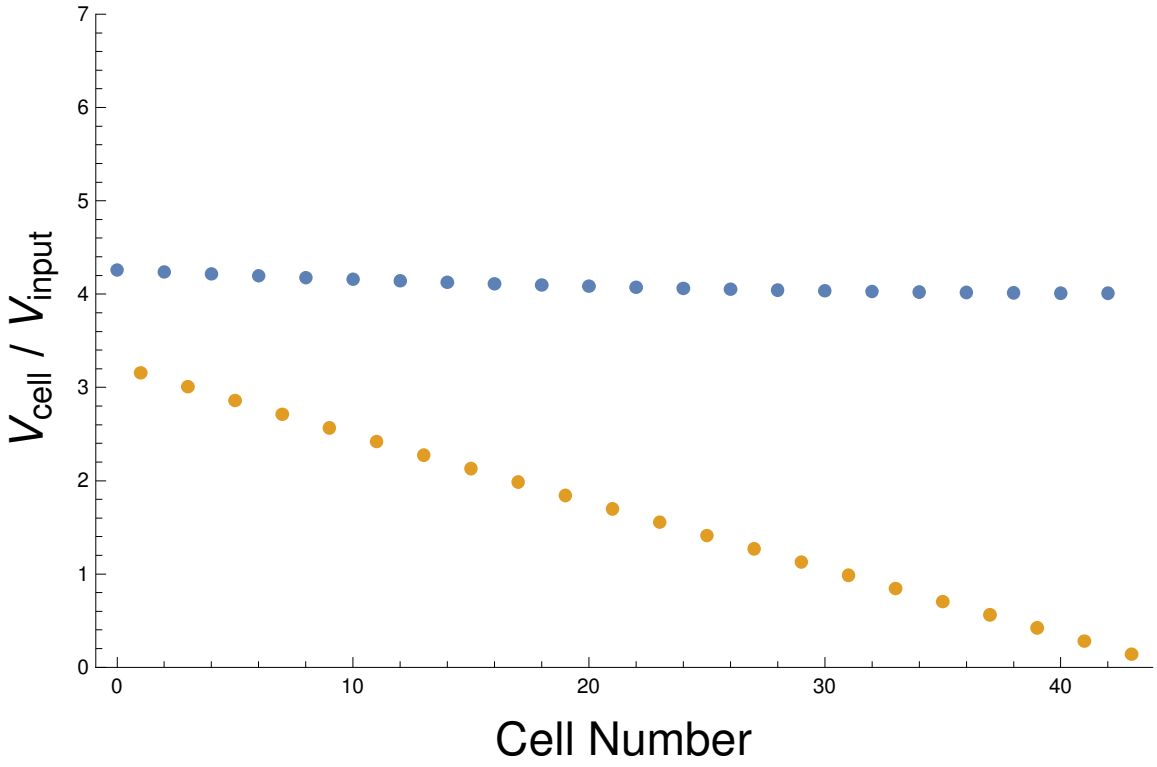

Figure 5.2: Spatial distribution of capacitor voltages for 45 cell resonant system operating in $\pi/2$ mode. Active cell voltages are shown in blue and coupling cell voltages are shown in yellow. Stored energy in active cells was adjusted so that the Q of each active cell equals 60 with design load applied. Coupling cell series resistance was adjusted to set the Q of each coupling cell to 300 to simulate small parasitic losses in coupling cell components.

Further details of the charging system such as optimal resonator frequency and stored energy, capacitor selection, and transformer design with core selection are left for future work. Other specifics relating to the Marx generator to be considered are: power takeoff and voltage regulation for gate drivers at each active cell, high frequency ac input power requirements and inverter design, system mechanical layout, and control system design. Specific considerations for driving the magnetron include power takeoff with regulation at the last active cell for the magnetron's cathode heater, magnetron voltage rate of rise window,

pulse voltage regulation, and arc interruption and other system protection features.

This example serves to demonstrate high power operation can be achieved with reasonable component values and illustrates a straightforward process for designing a system of resonantly coupled cascaded transformers for charging a Marx generator.

CHAPTER 6

SUMMARY

In Chapter 2 we considered an infinite biperiodic chain of coupled oscillations and derived the corresponding dispersion equation. We showed that unless the frequencies of the coupling cells and active cells are equal the structure will have a stopband corresponding to $\pi/2$ phase shift. Setting the two frequencies equal closes the stopband and allows waves to propagate with a $\pi/2$ phase shift and a non zero group velocity at a frequency independent of coupling. This insensitivity to coupling, non-zero group velocity, flat voltage distribution, and insensitivity to first order tuning errors led us to choose the $\pi/2$ as the operating mode for our resonant cascaded transformer structure.

In Chapter 3 we considered a finite system of coupled oscillators. Starting with Ohms law and Kirchhoff's voltage law we derive the corresponding eigenvector equation in terms of cell to cell coupling, cell inductance, cell capacitance, capacitor voltage, and angular frequency. Eigenvalues of this equation can be used to calculate the frequency of the modes of oscillation while the eigenvectors can be used to calculate the voltage distribution across the capacitors. By populating the matrices with the appropriate component values and using a computational math solver to solve for the eigenvectors and eigenvalues the properties of a finite system can be studied. In future studies this could be repeated for the equivalent circuit with resistive losses.

In the first section of Chapter 4 we discussed the construction of a bench top model composed of five cells, three active cells and two coupling cells. Component values were measured prior to assembly and used to calculate theoretical mode frequencies. After assembly the mode frequencies were measured and found to be in good agreement with the theoretical values. Spatial distribution of capacitor voltages was measured for each mode and found to be quite flat in the $\pi/2$ mode. Transient response of the voltage on the active cell capacitors were observed. The active cell capacitors were connected in series to demonstrate this did not interfere with the resonance of the system. Series connections were removed and voltage doubler circuits were added to each active cell resonant capacitor. The output of the doublers were connected in series to demonstrate high voltage dc could be generated. MOSFETs were added to the circuit to create a Marx generator and pulsed operation was demonstrated.

In the second section of Chapter 4 we built a model of the bench top circuit using the SPICE program Micro-Cap. The measured component values from the bench top system were used in the model. The model was analyzed in the frequency domain to determine mode frequencies. Simulated values for mode frequencies were in good agreement with those measured analytically. The simulated circuit was run in the time domain to observe transient response. MOSFETs were added to the simulated model and pules operation was simulated in the time domain.

In the final section of Chapter 4 we populated the matrix equation derived in Chapter 3 with the measured component values from the bench top model and calculated the mode frequencies. This demonstrated the application of the matrix equations to our circuit and served to validate the equation itself. The calculated mode frequencies were in good agrement with both the measured and the simulated values.

Having gained confidence in the tools developed, we move forward in Chapter 5 by

laying out the sketch of a Marx modulator charged via resonant cascaded transformers for a specific application, driving a MG7095 magneton. We started by looking at the voltage and power requirements of the magnetron. We choose the number of Marx stages based on the needed output voltage and voltage rating of currently available solid state switches and identified a possible IGBT switch. We picked the ratio of resonator peak voltage to Marx stage voltage and an operating frequency and loaded Q. We use these values to calculate the capacitance and inductance of our active cells. We pick the capacitance and inductance of our coupling cells to have the same resonant frequency as our active cells. We simulated this design in SPICE to observe its performance and found the voltage droop across the structure can be controlled through the design. Further work is needed, including selecting system parameters to minimize parasitic losses in capacitors and transformer cores, to create a fully specified design but feasibility was demonstrated.

Overall we have described and demonstrated the potential for charging Marx modulators via resonate cascaded transformers operating in the $\pi/2$ mode. We discussed several tools for the study of these resonant systems to aid with their design and discussed the construction of a small model to test these tools. A Marx generator charged in this way would have the same advantages of solid state Marx generators charged by other means such as construction from lower voltage modular subunits, design redundancy, short rise time, low series inductance, variable output pulse width and shape, ability to operate into different load impedances, and ability to operate into an open circuit and switch off in case of over current. The charging method discussed reduces or eliminates some of the difficulties with other charging methods such as low rep rate, capacitance from upper Marx stages to ground, and voltage distribution on charging switches. Further work is needed to explore the advantages and identify any shortcoming of this method of charging Marx generators and where its use is most appropriate. Work is also needed to explore optimal design parameters including

choices for resonant frequency, loaded Q, and coupling cavity characteristic impedance. The author hopes that the work contained herein will lead to further advancements in Marx generator technologies.

BIBLIOGRAPHY

[1] A. S. Gilmour, Jr. *Klystrons, Traveling Wave Tubes, Magnetrons, Crossed-Field Amplifiers, and Gyrotrons.* Artech House, Boston, 2011.

[2] M.A. Kemp. Solid state Marx modulators for emerging applications. SLAC-PUB-12235.

[3] G. N. Glasoe and J. V. Lebacqz. *Pulse Generators.* McGraw-Hill, first edition, 1948.

[4] H. Bluhm. *Pulsed Power Systems.* Springer, 2006.

[5] E. Marx. Verfahren zur Schlagprüfung von Isolatoren and anderen elektrischen Vorrichtungen, February 13, 1923. DE Patent 7,062,320.

[6] J. Lehr and C. Baum. Charging of Marx generators. Circuit and Electromagnetic System Design Notes Note 43, Air Force Research Laboratory, Directed Energy Directorate, June 2000.

[7] J. O'Loughlin, et al. High repetition rate charging a Marx type generator. In *Pulsed Power Plasma Science, 2001. PPPS-2001. Digest of Technical Papers*, Las Vegas, NV, USA, June 2001. IEEE.

[8] R. J. Adler and V. M. Weeks. Design and operation of a 700 kv arbitrary waveform generator. In *Pulsed Power Conference, 2009, IEEE*, page 3201, Washington, DC, USA, 2009.

[9] R. J. Richter-Sand, et al. Marx-stacked IGBT modulators for high voltage, high power applications. In *Power Modulator Symposium, 2002 and 2002 High-Voltage Workshop. Conference Record of the Twenty-Fifth International*, page 390, Hollywood, CA, USA, Jun. 2002.

[10] G. E. Lehy. Prototype development progress toward a 500 kV solid state Marx modulator. In *Power Electronics Specialists Conference, 2004. PESC 04. 2004 IEEE 35th Annual*, page 831, Aachen, Germany, Nov. 2004.

[11] H. Kirbie and G. Dale. Apparatus for producing voltage and current pulses, December 21 2010. US Patent 7,855,904 B2.

[12] Y. Wu, et al. Repetitive and high voltage Marx generator using solid-state devices. *IEEE Transactions on Dielectrics and Electrical Insulation*, 14(4):937, Aug 2007.

[13] S. Zabihi, et al. A solid-state Marx generator with a novel configuration. *IEEE Transactions on Plasma Science*, 39(8):1721, Jul. 2011.

[14] D. E. Nagle, at al. Coupled resonator model for standing wave accelerator tanks. *Rev. Sci. Instr.*, 38:1583, 1967.

[15] E. A. Knapp, et al. Standing wave high energy linear accelerator structures. *Rev. Sci. Instr.*, 39:979, 1968.

[16] H. A. Enge. Traveling wave high voltage generator, April 7 1970. US Patent 3,505,608.

[17] H. A. Enge. High voltage direct current generator, November 24 1970. US Patent 3,543,136.

[18] H. A. Enge. Cascad transformer high voltage generator, July 27 1971. US Patent 3,596,167.

[19] L. Brillouin. *Wave Propagation in Periodic Structures.* McGraw-Hill Book Company, 1946.

[20] T. Wangler. *RF Linear Accelerators.* John Wiley & Sones, New York, 1998.

[21] R. H. Potter, et al. Multiple coupled resonator power supply. In *2007 16th IEEE International Pulsed Power Conference*, volume 2, page 1635, 2007.

[22] R. H. Potter, et al. Multiple coupled resonator - applications to pulsed power. In *Proc. of 20th IET Symposium on Pulsed Power*, 2007.

[23] R. J. Adler. Pulsed power formulary. Print, Marana, AZ, January 2008.

[24] R. H. Potter, et al. High voltage generator with multiple inductive couplings, September 25 2012. US Patent 8,274,806.

[25] Spectrum Software. Micro-Cap 11. http://www.spectrum-soft.com/index.shtm. Accessed: 2017-10-26.

[26] Teledyne e2V. Mg7095. https://www.e2v.com/resources/account/download-datasheet/1948. Accessed: 2017-10-18.